Abstract

Ethnopharmacology relevance; The plant *Senecio nutans* SCh. Bip. is used by Andean communities to treat altitude sickness. Recent evidence suggests it may produce vasodilation and negative cardiac inotropy, though the cellular mechanisms have not been elucidated.
Purpose: To determinate the mechanisms action of *S. nutans* on cardiovascular function in normotensive animals.
Methods: The effect of the extract on rat blood pressure was measured with a transducer in the carotid artery and intraventricular pressure by a Langendorff system. The effects on sheep ventricular intracellular calcium handling and contractility were evaluated using photometry. Ultra-high-performance liquid-chromatography with diode array detection coupled with heated electrospray-ionization quadrupole-orbitrap mass spectrometric detection (UHPLC-DAD-ESI-Q-OT-MSn) was used for extract chemical characterization.
Results: In normotensive rats, *S. nutans* (10 mg/Kg) reduced mean arterial pressure (MAP) by 40 % ($p < 0.05$), causing a dose-dependent coronary artery dilation and decreased left ventricular pressure. In isolated cells, *S. nutans* extract (1 µg/ml) rapidly reduced the $[Ca^{2+}]_i$ transient amplitude and sarcomere shorting by 40 and 49 % ($p<0.001$), respectively. The amplitude of the caffeine evoked $[Ca^{2+}]_i$ transient was reduced by 24 % ($p<0.001$), indicating reduced sarcoplasmic reticulum (SR) Ca^{2+} content. Sodium-calcium exchanger (NCX) activity increased by 17 % ($p<0.05$), while sarcoendoplasmic reticulum Ca^{2+}-ATPase (SERCA) activity was decreased by 21 % ($p<0.05$). LC-MS results showed the presence of vitamin C, malic acid, and several antioxidant phenolic acids reported for the first time. Dihydroeuparin and 4-hydroxy-3-(3-methylbut-2-enyl) acetophenone were abundant in the extract.
Conclusion: In normotensive animals, *S. nutans* partially reduces MAP by decreasing heart rate and cardiac contractility. This negative inotropy is accounted for by decreased SERCA activity and increased NCX activity which reduces SR Ca^{2+} content. These results highlight the plant's potential as a source of novel cardio-active phytopharmaceuticals or nutraceuticals.

Keywords: Cardiac function; contractility; endemic plants; intracellular calcium; mass spectrometry; myocyte.

Graphical Abstract

A Hydroalcoholic Extract of *Senecio nutans* SCh. Bip (Asteraceae); its effects on cardiac function and chemical characterization

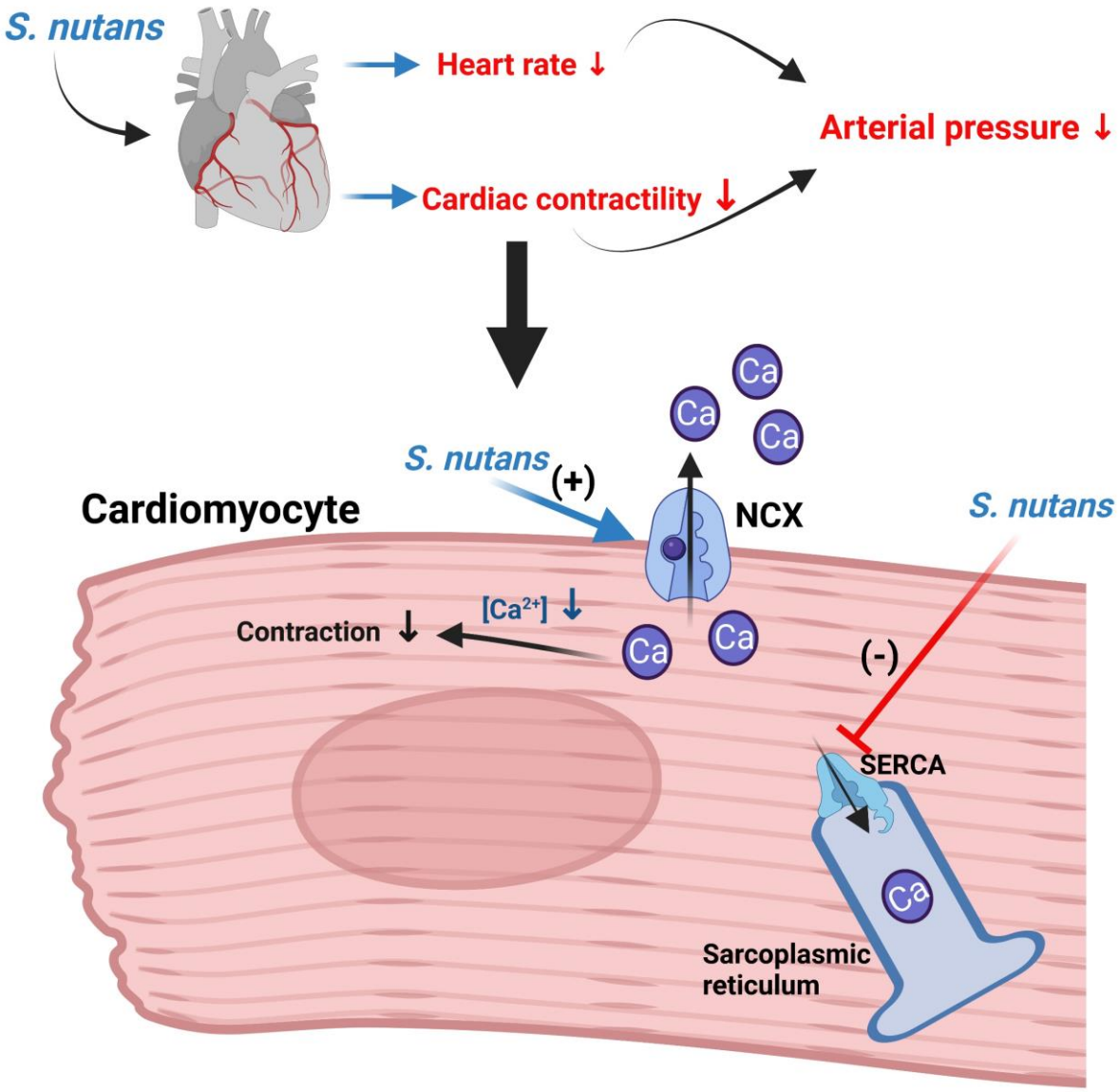

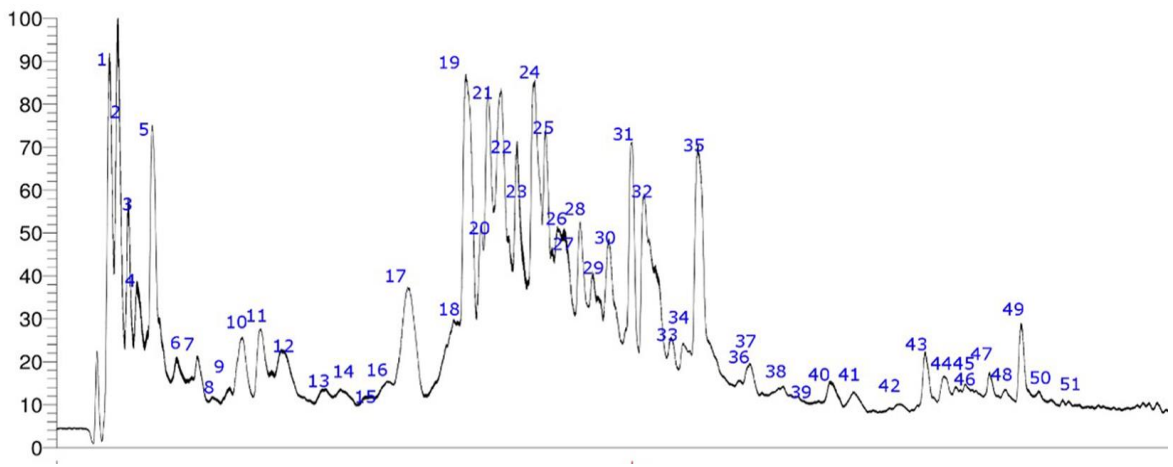

A Hydroalcoholic Extract of *Senecio nutans* SCh. Bip (Asteraceae); its effects on cardiac function and chemical characterization

Javier Palacios[a*], Adrián Paredes[b,c], Fredi Cifuentes[c,d], Marcelo A. Catalán[e], Angel Luis García-Villalón[f], Jorge Borquez[b], Mario J. Simirgiotis[g], Matthew Jones[h], Amy Foster[h], David J. Greensmith[h*]

[a] Laboratorio de Bioquímica Aplicada, Química y Farmacia, Facultad de Ciencias de la Salud, Universidad Arturo Prat, Iquique 1110939, Chile. clpalaci@unap.cl (J.P.)

[b] Departamento de Química, Facultad de Ciencias Básicas, Universidad de Antofagasta, Antofagasta 1271155, Chile. adrian.paredes@uantof.cl (A.P.), jorge.borquez@uantof.cl (J.B.)

[c] Instituto Antofagasta (IA), Universidad de Antofagasta, Antofagasta 1271155, Chile

[d] Departamento de Biomédico, Facultad Ciencias de la Salud, Universidad de Antofagasta, Antofagasta 1271155, Chile. fredi.cifuentes@uantof.cl (F.C.)

[e] Instituto de Fisiología, Facultad de Medicina, Universidad Austral de Chile, Valdivia 5090000, Chile. marcelo.catalan@uach.cl (M.A.C.)

[f] Departamento de Fisiología, Facultad de Medicina, Universidad Autónoma de Madrid, 28029 Madrid, Spain. angeluis.villalon@uam.es (A.L.GV.)

[g] Center for Interdisciplinary Studies on the Nervous System (CISNe), Universidad Austral de Chile, Valdivia, 5090000, Chile. simirgiotis@gmail.com (M.J.S.)

[h] Biomedical Research Centre, School of Science, Engineering and Environment, The University of Salford, Salford, United Kingdom. M.A.Jones9@salford.ac.uk (M.J.), A.Foster6@edu.salford.ac.uk (A.F.), d.j.greensmith@salford.ac.uk (D.J.G.)

[*]Corresponding author: clpalaci@unap.cl +56-57-2526910 (J.P.) and d.j.greensmith@salford.ac.uk +44 1612952170 (D.J.G.)

Abstract

Ethnopharmacology relevance; The plant *Senecio nutans* SCh. Bip. is used by Andean communities to treat altitude sickness. Recent evidence suggests it may produce vasodilation and negative cardiac inotropy, though the cellular mechanisms have not been elucidated.
Purpose: To determinate the mechanisms action of *S. nutans* on cardiovascular function in normotensive animals.
Methods: The effect of the extract on rat blood pressure was measured with a transducer in the carotid artery and intraventricular pressure by a Langendorff system. The effects on sheep ventricular intracellular calcium handling and contractility were evaluated using photometry. Ultra-high-performance liquid-chromatography with diode array detection coupled with heated electrospray-ionization quadrupole-orbitrap mass spectrometric detection (UHPLC-DAD-ESI-Q-OT-MSn) was used for extract chemical characterization.
Results: In normotensive rats, *S. nutans* (10 mg/Kg) reduced mean arterial pressure (MAP) by 40 % ($p < 0.05$), causing a dose-dependent coronary artery dilation and decreased left ventricular pressure. In isolated cells, *S. nutans* extract (1 µg/ml) rapidly reduced the $[Ca^{2+}]_i$ transient amplitude and sarcomere shorting by 40 and 49 % ($p<0.001$), respectively. The amplitude of the caffeine evoked $[Ca^{2+}]_i$ transient was reduced by 24 % ($p<0.001$), indicating reduced sarcoplasmic reticulum (SR) Ca^{2+} content. Sodium-calcium exchanger (NCX) activity increased by 17 % ($p<0.05$), while sarcoendoplasmic reticulum Ca^{2+}-ATPase (SERCA) activity was decreased by 21 % ($p<0.05$). LC-MS results showed the presence of vitamin C, malic acid, and several antioxidant phenolic acids reported for the first time. Dihydroeuparin and 4-hydroxy-3-(3-methylbut-2-enyl) acetophenone were abundant in the extract.
Conclusion: In normotensive animals, *S. nutans* partially reduces MAP by decreasing heart rate and cardiac contractility. This negative inotropy is accounted for by decreased SERCA activity and increased NCX activity which reduces SR Ca^{2+} content. These results highlight the plant's potential as a source of novel cardio-active phytopharmaceuticals or nutraceuticals.

Keywords: Cardiac function; contractility; endemic plants; intracellular calcium; mass spectrometry; myocyte.

Introduction

Senecio nutans (Sch.) Bip. (Synonyms: *Senecio graveolens* Wedd, *Senecio graveolens var. Psiloachaenius* Cabrera) is a perennial shrub approximately 20-60 cm high that grows in the Andes of Chile, Argentina, Perú, and Bolivia at 3500-5000 m.a.s.l. (Villagrán et al., 2003). It belongs to the family Asteraceae and a group of medicinal plants colloquially known as "Chachacoma".

Previous studies on this plant reported the presence of several exciting acetophenones (Loyola et al., 1985), which were bioactive compounds for altitude sickness and possessed cytotoxic activity (Cifuentes et al., 2016; Echiburú-Chau et al., 2014).

Our previous work revealed extracts of *S.nutans* exhibit hypotensive properties in normotensive rats and mice (Fredi Cifuentes et al., 2016). Here, extracts decreased heart rate (HR) and prolonged corrected QT (QTc). This bradycardia maybe due to reduced sino-atrial node activity as indicated by experiments using the isolated right atrium of normotensive rats (Fredi Cifuentes et al., 2016). Interestingly, the cardiovascular effect of *S. nutans* were similar to those displayed by Ca^{2+} channel blockers such as nifedipine, which decreases the frequency of beats of the right atrium and papillary muscle contractility of the left ventricle of. Furthermore, we demonstrated a direct negatively inotropic effect in intact hearts (Fredi Cifuentes et al., 2016), though the cellular basis of this phenomenon remains unknown.

In other work, we found *S. nutans* promotes vasodilation via Ca^{2+} and nitric oxide-dependent mechanisms (Paredes et al., 2016). Here, pre-incubation of intact aortic rings with *S. nutans* extracts reduced the contractile response to phenylephrine (PE) by blocking inward Ca^{2+} currents (Paredes et al., 2016).

Collectively, this evidence suggests *S. nutans* may be of value as a hypotensive agent. Despite this, an investigation of the cardiac cellular effects, or detailed metabolome analysis of the bioactive hydroalcoholic extract has yet to be reported. Therefore, the objective of the present study was to determine the mechanism of action of *S. nutans* on cardiovascular function in normotensive animals. We investigated (1) the hypotensive actions of *S. nutans in vivo*; (2) the cellular basis of the negative cardiac inotropy; and (3) the phytochemical fingerprint (UHPLC-DAD-ESI-Q-OT-MS) of *S. nutans*

Materials and Methods

Plant Material

S. nutans Sch. Bip was collected in the village of Toconce (22°15'11.16'' S, 68°5'44.68'' W, at 3,788 m.a.s.l.), North of Chile, Antofagasta Region. Dr. Roberto Rodríguez, Universidad de Concepción, Chile identified the plant (herbarium for collection; voucher # CONC 139.929).

Extraction preparation

The plant material (aerial parts) was ground and dried at room temperature. The powdered plant (2 Kg dry) was put into a cotton bag and immersed in 4 L of a mixture of EtOH: H_2O (1:1). After 72 h at room temperature, the solution was filtered (Whatman Nº 4) and concentrated on a rotary evaporator (50° C), and the result was a quarter of the initial volume. We repeated this method several times to obtain a final colorless solution. The lyophilized hydroalcoholic extract was stored at 4°C until use. The extraction yield was 19%.

Animals

Experiments on isolated hearts (Langendorff system) used male Sprague Dawley rats (6–8 weeks old; 170–200 g). The animals were randomized and housed at a room temperature of 22–25 °C in a light/dark photoperiod (12 hours each, lights were turned on at 8:00 am and turned off at 08:00 pm). The animal had *ad libitum* access to water and food (Champion, Santiago). Two groups of normotensive male rats were used in this study; group 1 (n = 5) for blood pressure protocol and group 2 for Langendorff protocol (n = 5). The animal research committee of Antofagasta University approved the experimental protocol (CEIC #275/2020). Experiments on cells used Welsh sheep by the Animals (Scientific Procedures) Act, UK, 1986, Directive 2010/63/EU of the European Parliament and local ethical review boards.

Blood pressure and heart rate measurements

As described in a previous study, MAP and HR were measured in rats (F Cifuentes et al., 2018). The rats were anesthetized with ketamine (42 mg/Kg, i.p.) and xylazine (5 mg/Kg, i.p.). We measured the blood pressure in the carotid artery and administered the extract (5, 10, 20, and 40 mg/Kg of body weight) through the saphenous vein. The doses of the extract were based on our previous study (Fredi Cifuentes et al., 2016). In that study, we found that 40 mg/Kg of body weight reduced the increase in blood pressure induced by angiotensin II. Therefore, doses below 40 mg/Kg were the focus of this physiological study.

Langendorff isolated the heart system

Briefly, animals were anesthetized, and the heart was quickly removed and mounted on the Langendorff system (constant flow of 10 mL/min of buffer). Krebs-Henseleit buffer (KHB) contains (in mM); 4.7 KCl, 1.2 KH_2PO_4, 118 NaCl, 25 Na_2HCO_3, 1.2 $MgSO_4$, 1.75 $CaCl_2$, 0.5 EDTA and 8 D-glucose (pH 7.4; 37°C; 95% O_2 and 5% CO_2). A ball of polyvinyl was inserted into the left ventricle and filled with 0.9% NaCl solution to measure contractile function. The heart was perfused with extract (1, 10, 100, 300, or 1000 μg/mL). The doses used in the extract for the Langendorff protocol were the same used in vascular reactivity experiments previously reported (Paredes et al., 2016). In this case, we found that 100 μg/mL extract caused a significant relaxation of rat aorta. The PoweLab8 system (ADInstruments, Australia) was used.

Intracellular Ca^{2+} and contractility measurements in isolated sheep ventricular myocytes.

Sheep ventricular myocytes were enzymatically isolated - by retrograde perfusion of the coronary arteries with collagenase and protease - as previously described (Greensmith et al., 2014a) and then loaded with the acetoxymethyl ester (AM) form of fura–2 (1 μM) for 10 min at room temperature. During Ca^{2+} measurements, cells were field stimulated at 0.5 Hz and perfused (37 °C) with a solution containing (in mM): NaCl 140, HEPES 10, glucose 10, KCl 4, probenecid 2, $MgCl_2$ 1, $CaCl_2$ 1.8, pH 7.35 with NaOH. The probenecid prevents loss of fura–2 from the cell at 37°C. Fura–2 was excited sequentially (200 Hz) at 340 and 380 nm using OptoLED light sources (Cairn Research, UK). Emitted fluorescence was measured via a 515 nm long-pass filter using a photomultiplier tube coupled to a photometry system (Cairn Research UK). Changes in cytoplasmic Ca^{2+} were inferred from the ratio of light emitted at

340:380 nm, calibrated using custom-written software (Greensmith, 2014). Cell contractility was evaluated simultaneously by measuring sarcomere length using a MyoCamS high-speed camera and SarcLen acquisition module (Ion Optix, USA).

Measurement of SR Ca^{2+} content and the activity of the Ca^{2+} removal mechanisms

Relative changes to Sarcoplasmic Reticulum (SR) Ca^{2+} content were measured by comparing the amplitude of Ca^{2+} transients evoked by applying 10 mM caffeine which causes rapid emptying of the SR. The descending phase of the systolic Ca^{2+} transient was fitted with a single exponential decay (Greensmith, 2014). Here, the rate constant of decay (k_{sys}) depends on the combined activity of the Sarco-Endoplasmic Reticulum Ca^{2+} ATPase (SERCA) and Sodium-Calcium Exchanger (NCX), whereas that of the caffeine evoked Ca^{2+} transient (k_{caff}) predominantly depends on NCX. Subtracting these rate constants gives k_{SERCA} and a calculated indication of SERCA activity.

UHPLC-DAD-ESI-Q-OT-MSn Instrument

Liquid chromatography (UHPLC-diode array- electrospray ionization- quadrupole orbitrap high-resolution-mass spectrometry) was performed as described in **Supplementary Information.**

Chemicals

Sephadex LH-20 was bough to Pharmacia Fine Chemicals (Piscataway, NJ, USA). While the following substances were obtained from Merck (Santiago, Chile); acetonitrile, methanol, hexane, and ethyl acetate.

Statistical Analysis

SEM (mean ± standard error of the mean) was used in this study. One-way ANOVA and one-way RM ANOVA were used to analyze statistically the data, followed by *post hoc* Bonferroni or Tukey tests. Graph Pad Prism, version 5.0. (GraphPad Software, Inc., La Jolla, CA, USA) and SigmaPlot version 12.0 (Systat Software Inc, USA) was used. A $p < 0.05$ was considered statistically different.

Results

The hydroalcoholic extract from S. nutans causes a hypotensive effect in rats.

We measured in vivo arterial blood pressure in anesthetized rats to determine whether our results may have clinical implications. MAP started to decrease at 10 mg/Kg of *S. nutans* extract: 130 ± 4 mmHg basal versus 75 ± 5 mmHg with 10 mg/Kg extract ($P< 0.01$; **Fig. 1A**). However, HR decreased at 40 mg/Kg extract (289 ± 7 bpm basal versus 231 ± 9 bpm with extract; $P < 0.01$; **Fig. 1B**).

S. nutans decrease the coronary pressure and the cardiac contractility in the Langendorff system.

The coronary and left ventricular pressure (LVP) were measured to gain insight into the extract's role in cardiac function. In the first Langendorff protocol, the cardiac contractility was determined while the heart rate was kept constant (360 bpm). *S. nutans* decreased the coronary pressure significantly ($P < 0.05$): 54 ± 6 mmHg basal versus 25 ± 11 mmHg with 100 μg/mL (**Fig. 2A**). While the LVP slightly decreased at the same extract concentration (75 ± 6 mmHg basal versus 44 ± 18 mmHg with 100 μg/mL), and it was abolished at 1000 μg/mL, **Fig. 2B**). After washing out, the LVP partially recovered (22 ± 13 mmHg). Since coronary and LV pressure did not completely recover during washout following exposure to 1000 μg/ml, we reduced the dose to 300 μg/ml.

In the second protocol, we allowed the heart to beat freely. Again, the coronary pressure decreased significantly in dose-dependent way, 67 ± 1 mmHg basal versus 62 ± 1 mmHg at 10 μg/mL ($P<0.05$), 60 ± 1 mmHg at 100 μg/mL ($P< 0.01$), and 50 ± 2 mmHg at 300 μg/mL ($P<0.001$) (**Fig. 2C**). In this protocol, the HR increased (192 ± 5 bpm basal versus 215 ± 6 bpm with 300 μg/mL) when coronary pressure decreased, but statistical analysis did not show significance (**Fig. 2D**). Here, we did not observe a reduction in LVP at all (data not shown).

The effects of S. nutans on cardiac intracellular Ca^{2+} and contractility dynamics in isolated cardiac myocytes

To evaluate whether changes to cell function contribute to the effects observed in isolated hearts, we next measured the effect on intracellular calcium ($[Ca^{2+}]_i$) and contractility dynamics on isolated cardiac myocytes. The sheep was chosen as the study model as (1) they are particularly convenient for the photometric methods used in this study, (2) for alignment

to 3Rs principles and (3) because the fundamental cardiac cellular physiology of sheep is similar to that of rat. *S. nutans* extracts (0.01, 0.1, 1, 10 and 100 µg/ml) produced a concentration-dependent decrease in both the Ca^{2+} transient amplitude and systolic shortening (**Fig. 3**). A 1 µg/ml concentration was used for all subsequent detailed analyses.

The experiment represented in **Fig. 4A** and **D** (representative of data from 24 cells) shows that application of 1 µg / ml S. *nutans extract* rapidly (10-20 s) decreased the amplitude and rate of decay of the $[Ca^{2+}]_i$ transient to a lower steady state. On average, systolic Ca^{2+} (**Fig. 4B**) was reduced by 40 ± 4 % ($p < 0.001$) which partially reversed to 69 ± 8 % ($p = 0.02$) of control upon washout. Diastolic $[Ca^{2+}]_i$ (**Fig. 4C**) progressively decreased during the experiment to 93 ± 3 % ($p = 0.04$) of control by the end of washout. The rate constant of systolic Ca^{2+} decay (k_{sys}, **Fig 4E**) was reduced by 17 ± 4 % ($p = 0.002$), which reversed to levels equivalent to control on washout.

The experiment represented in **Fig. 5A** shows the associated effect on cell contractility. On average, systolic sarcomere shortening (**Fig 5B**) was reduced by 49 ± 4 % ($p < 0.001$). Diastolic sarcomere length (**Fig 5C**) was unaltered, and while an increase in relaxation rate (**Fig 5D**) was apparent, this did not reach significance. To determine the dependence of sarcomere length on $[Ca^{2+}]_i$, phase plane analysis was performed. **Fig. 5E** shows that the slope of sarcomere length versus $[Ca^{2+}]_i$ was reduced by 28 ± 8 % ($p = 0.02$) and then reversed on washout.

The effects of S. nutans on SR Ca^{2+} content and systolic Ca^{2+} removal pathways

The experiment represented in **Fig. 6A** (representative of data from 13 cells) shows that application of 1 µg / ml S. *nutans extracts* decreased the amplitude of caffeine-evoked $[Ca^{2+}]_i$ transients indicating a relative decrease in SR Ca^{2+} content. On average, relative SR Ca^{2+} content (**Fig 6B**) was decreased by 24 ± 4 % ($p < 0.001$) which progressed to 41 ± 6 % ($p < 0.001$) during washout. The rate of Ca^{2+} removal was determined to understand the cause of the decrease of SR Ca^{2+} content. The rate constant of decay of the caffeine induced $[Ca^{2+}]_i$ transient (k_{caff}) (**Fig. 6C**) was increased by 17 ± 4 % ($p = 0.04$), progressing to 41 ± 7 % ($p < 0.001$) during washout and indicating associated increases of NCX activity. The SERCA activity was calculated as $k_{SERCA} = k_{sys} - k_{caff}$ and was decreased by 21 ± 8 % ($p = 0.02$) and then reversed on washout (**Fig. 6D**).

High-Resolution UHPLC-DAD-ESI-Q-Orbitrap-Mass Spectrometry Analysis

The analysis of the phenolic composition of *S. nutans* was carried out by UHPLC-DAD-ESI-Q-OT-MS using four detection channels (330, 280, 254, and 440 nm, plus 3D DAD plotting) and the negative heated ionization mode (HESI-II). The total ion current and Photodiode-Array Detection (PDA) chromatograms of the hydroalcoholic extract are shown in **Fig. 7**.

Firstly, the phenolic compounds were identified by the analysis of each ultraviolet (UV) spectra. Involves the determination of the molecular weight of each molecule and the analysis of the daughter ions (MS^n) detected for each parent molecule. The most intense peak corresponds to the deprotonated molecular ion $[M-H]^-$, followed by some $[2M-H]^-$ diagnostic adducts ions and some MS^n daughter ions in the negative ionization mode (HESI-II^-) MS^1 spectrum. The MS^n profiles of the detected molecules are shown in **Table S1 and Fig. S1,** and the characterization of the compounds follows below. In **Supplementary Fig. S2**, the tentative derivatives detected in *S. nutans* extract.

Simple organic acids

Peaks 2, 3, and 4 with molecular anions at m/z: 191.05611, 133.01425, 191.01973 were identified as quinic, malic, and citric acids ($C_7H_{11}O_6^-$, $C_4H_5O_5^-$ and $C_6H_7O_7^-$) (Brito et al., 2014; Echiburu-Chau et al., 2017), respectively.

Aminoacids

In positive mode, several underivatized amino acids were detected in *S. nutans* extract using the quadrupole-orbitrap analyzer (Le et al., 2014; Nemkov et al., 2015). Peak 1 with a molecular cation at m/z: 147.07695 was identified as glutamine ($C_5H_{11}O_3N_2^+$) and peak 6 as leucine or isoleucine ($C_6H_{14}O_2N^+$), Peak 10 as phenylalanine ($C_9H_{12}O_2N^+$) and peak 13 as asparagine ($C_4H_9O_3N_2^+$). Similarly, peak 16 with molecular cation at m/z: 205.09784 was identified as tryptophan ($C_{11}H_{13}O_2N_2^+$).

Acetophenones and related compounds

Peak 7 with an ion [M-H]- at m/z: 329.08795 was regarded as the glycoside 3,4-dihydroxyacetophenone 5-O-glucoside, ($C_{14}H_{17}O_9^-$), Peak 28 with an ion $[M-H]^-$ at *m/z*: 413.18198 as the *glycosyl* derivative: 3-methoxy-4-hydroxy-5-(3-methyl-2-butyl)

acetophenone 2-O-glucoside ($C_{20}H_{29}O_9^-$). In the same manner, peak 26 with an ion $[M-H]^-$ at *m/z*: 381.15561 was identified as 2-O-glucosyl-4-hydroxy-5-(3-methyl-2-butenyl) acetophenone ($C_{19}H_{25}O_8^-$), peak 27 with an ion $[M-H]^-$ at *m/z*: 411.16626 was tentatively characterized as another glycosyl derivative: 3-methoxy-4-hydroxy-5-(3-methyl-2-butenyl) acetophenone, 2-O-glucoside ($C_{20}H_{27}O_9^-$), peak 28 as 2-O-glucosyl-3-methoxy-4-hydroxy-5-(3-methyl-2-butyl) acetophenone ($C_{20}H_{29}O_9^-$) peak 32 was assigned to the reduced benzofurane and UV ray absorbent-sunscreen molecule dihydroeuparin (*m/z*: 217.08676, $C_{13}H_{13}O_3^-$) (Ortega et al., 2000; Tang et al., 1987), while peak 38 with a pseudo-molecular ion at *m/z*: 219.10242 as 2,4-dihydroxy-5-(3-methyl-2-butenyl) acetophenone ($C_{13}H_{15}O_3^-$). In the same manner, peak 37 (parent ion at *m/z*: 221.11983) was identified as the isomer of the later, 4-hydroxy-3-(1-en-3-methyl-3-butanol) acetophenone ($C_{13}H_{15}O_3^-$), Peak 40 with a parent ion at *m/z*: 249.11327 was identified as 5-acetyl-2,3-dihydro-6-hydroxy-7-methoxy-2-(isopropenyl)benzofurane ($C_{14}H_{17}O_4^+$) peak 4<2 with a pseudomolecular ion at *m/z*: 237.11334 was characterized as 5-acetyl-2,3-dihydro-6-hydroxy-2-(1-methyl-1-hydroxyetane)benzofurane ($C_{13}H_{17}O_4^+$). Finally, peak 31 with an ion $[M-H]^-$ at *m/z*: 203.10744 was identified as 4-hydroxy-3-(3-methyl-2-butenyl) acetophenone ($C_{13}H_{15}O_2^-$) and peak 47 as the non-substituted core structure acetophenone ($C_8H_9O^+$).

Phenolic acids

Several compounds were detected mainly in negative mode as phenolic acids. Peak 12 with an ion $[M-H]^-$ at *m/z*: 343.10361 was labeled as dehydro-caffeoyl-beta-D-glucopyranoside ($C_{15}H_{19}O_9^-$); these compounds have many bioactive effects, including acetylcholinesterase inhibition (Wang et al., 2017) and inhibition of the development of platelet aggregation and amplification of platelet activation (Fu et al., 2017), while peak 14 with an ion $[M-H]^-$ at *m/z*: 341.08795 was tentatively labeled as caffeoyl-beta-D-glucopyranoside ($C_{15}H_{17}O_9^-$). Accordingly, peak 19 with an ion $[M-H]^-$ at *m/z*: 383.09860 was identified as an acetylated caffeoyl-beta-D-glucopyranoside ($C_{17}H_{19}O_{10}^-$), while peak 24 with a pseudo-molecular ion at *m/z*: 367.10364 was regarded as 5-O-feruloylquinic acid ($C_{17}H_{19}O_9^-$), which was reported active against yeast glucosidase (Chen et al., 2014), peak 34 as *p*-coumaric acid ($C_9H_7O_3^-$), peak 25 with a molecular anion at *m/z*: 179.03471 was identified as caffeic acid ($C_9H_7O_3^-$), peaks 17 with pseudo-molecular ions at *m/z*: 515.11959 and daughter caffeoyl quinic ion at *m/z*: 353.08781 was identified as one of the isomers of dicaffeoylquinic acid ($C_{25}H_{23}O_{12}^-$),

peak 35 as chlorogenic acid, (*m/z*: 353.08798) peak 39 as 3-methyl-4-methoxycinnamic acid ($C_{11}H_{11}O_3^-$), peak 34 as coumaric acid ($C_9H_7O_3^-$) and peak 36 as cinnamic acid (*m/z*: 147.04454, $C_9H_7O_2^-$). These caffeoyl and feruloyl quinic acid derivatives have displayed previously anti-diabetic activity (Chen et al., 2014).

Oxylipins

Fatty acid components of healthy food such as asparagus are known as oxylipins; these important dietary compounds possess high antioxidant activity (Jiménez-Sánchez et al., 2016) and some antifungal activity (Martin-Arjol et al., 2010). Accordingly, peak 18 was identified as a glycosyl fatty acid conjugate, tetrahydroxydodecaenoic acid-O-glucoside ($C_{18}H_{31}O_{12}^-$). In the same manner, peak 5 was characterized in positive mode as the amino fatty acid derivative amineoxodecanoic acid ($C_{10}H_{20}O_3N^+$) (Kuno et al., 2015), peak 8 with a pseudomolecular cation at *m/z*: 174.14940 as amine-nonanoic acid ($C_9H_{20}O_2N^+$) and peak 9 with molecular cation at *m/z*: 160.13373 as aminoctanoic acid ($C_8H_{18}O_2N^+$). Peak 11 was assigned as the saturated small 8 carbons fatty acid caprylic acid ($C_8H_{17}O_2^+$). Finally, peaks 41 with an ion $[M-H]^-$ at *m/z*: 327.21793 was identified as trihydroxyoctadecadienoic acid ($C_{18}H_{31}O_5^-$) (Martin-Arjol et al., 2010) and peak 44 with 2 more hydrogens and an ion $[M-H]^-$ at *m/z*: 329.23346 as trihydroxyoctadecaenoic acid ($C_{18}H_{33}O_5^-$).

Flavonoids

Some compounds were characterized as quercetin or myricetin derivatives, peaks 43 and 51 (λ max: 254 and 354 nm) with molecular anions at *m/z*: 345.06171 and 343.08258 were characterized as: 3', 7-dimethoxymyricetin (Echiburu-Chau et al., 2017) and 7,4', 5'-trimethoxyquercetin, ($C_{17}H_{13}O_8^-$ and $C_{18}H_{15}O_7^-$), respectively. Peak 15 with an ion $[M-H]^-$ at *m/z*: 493.09885 was identified as a flavonol glycoside derivative: 7-methoxymyricetin 3-O-glucoside ($C_{22}H_{21}O_{13}^-$) and peak 29 with an ion $[M-H]^-$ at *m/z*: 549.12488 as its acetylated derivative: 7-acetyl-3-O-glucoside-3',4'-dimethoxymyricetin ($C_{25}H_{25}O_{14}^-$) while peak 22 with a ion $[M-H]^-$ at *m/z*: 491.11966 was characterized as 7,3'-dimethoxyquercetin 3-O-glucose ($C_{23}H_{23}O_{12}^-$). Peak 21 with a ion $[M-H]^-$ at *m/z*: 579.14819 was identified in positive mode as 5,6,7,4' -tetrahydroxyflavone-7-O-cynammoyl-glucose ($C_{30}H_{27}O_{12}^+$) and peak 20 as 5,6,7,4'-tetrahydroxyflavone-7-O-coumaroyl-glucose ($C_{30}H_{27}O_{13}^+$), while peak 23 with an ion $[M-H]^-$ at *m/z*: 507.11447 as: 3-O-glucosyl-3',4'-dimethoxymyricetin ($C_{23}H_{23}O_{13}^-$).

Coumarins

Peaks 45, 46, 48-50 were identified as coumarins (Simirgiotis et al., 2013b). The simple coumarin compound peak 45 was detected in positive mode (ion at *m/z*: 147.04446, $C_9H_7O_2^+$), while peak 49 was determined as umbelliferone ($C_9H_7O_3^+$) and peak 50 as scopoletin ($C_{10}H_9O_4^+$). Peak 30 with a pseudomolecular ion at *m/z*: 209.04518 was characterized as 8-hydroxyescopoletin or aesculetin ($C_{10}H_9O_5^+$) (Simirgiotis et al., 2013b), peak 33 as hydroxy-3-(1-en-3-methyl-3-butanol) acetophenone, peak 48 as herniatin ($C_{10}H_9O_3^+$) and peak 46 as 8-hydroxy-7-methoxy-scopoletin ($C_{11}H_{11}O_5^+$) (Echiburu-Chau et al., 2017) and peak 47 as acetophenone.

Discussion

This study, for the first time, showed the hypotensive properties of the hydroalcoholic extract of *Senecio nutans* are related to altered $[Ca^{2+}]_i$ handling and contractility in isolated cardiac myocytes.

Effect of S. nutans on blood pressure and isolated heart Langendorff

The extract was administered to anesthetic normotensive rats to assess whether *S. nutans* may have clinical consequences. The reduction in MAP would cause a decrease in HR and cardiac contractility. In a previous study, we demonstrated that oral extract administration for ten days in rats or intravenous administration in mice reduced the MAP (Fredi Cifuentes et al., 2016).

Notably, our results show that *S. nutans* caused coronary artery dilation in a dose-dependent way under both protocols; when the HR held constant at 360 bpm, or the heart was allowed to beat freely. The negative inotropic effect of *S. nutans* could explain by a lower peripheral vascular resistance. This hypothesis is supported because the extract caused coronary vasodilation, leading to a reduction in afterload (peripheral vascular resistance; (Khatib and Wilson, 2018) and an increase of the heart to preload as a function of afterload (Schotola et al., 2017).

In the second Langendorff protocol – where the heart was allowed to beat freely - an increase in the HR was observed while the coronary arteries dilated in the presence of *S. nutans*. Since the left ventricular pressure did not decrease (data not shown), we assume that the contractility of the heart did not change either. Therefore, it is possible that increased HR counteracted the effect of coronary artery dilatation on the decrease in afterload and blood pressure (LaCombe and Lappin, 2020).

This study showed a slight decrease of inotropic at submaximal doses of extract and significant reduction with maximal doses. However, in a previous study, we clarified that extract a significantly decreased ventricular contractility at submaximal doses in rat (F Cifuentes et al., 2016).

The effects of S. nutans on intracellular Ca^{2+} handling and contractility

To provide a cellular basis for the ventricular negative inotropy observed in the current and our previous study (F Cifuentes et al., 2016), we evaluated the effect of the extract on $[Ca^{2+}]_i$ and contractility in isolated myocytes. *S. nutans* decreases the $[Ca^{2+}]_i$ transient amplitude, accounting for reduced systolic shortening (Bers, 2002). The amplitude of the $[Ca^{2+}]_i$ transient is proportional to the third power of the SR Ca^{2+} content (Dibb et al., 2007). *S. nutans* reduced SR Ca^{2+} content to 76 % of control. This would be expected to decrease the $[Ca^{2+}]_i$ transient to $(0.76)^3 = 44$ %. The Ca^{2+} transient only decreased to 60 %, indicating that the decreased SR Ca^{2+} is more than enough to account for the $[Ca^{2+}]_i$ transient amplitude. We acknowledge, however, that we do not know if extracts of *S. nutans* alter Ca^{2+} buffering; thus, the relationship between total SR Ca^{2+} release and free Ca^{2+} (to which fura–2 fluorescence is proportional), so it is not possible to quantify the absolute change of SR Ca^{2+} content (Trafford et al., 1999; Varro et al., 1993). Indeed, this may explain why SR Ca^{2+} content progressively decreases during washout while the $[Ca^{2+}]_i$ partially recovers. Nonetheless, the *relative* change of caffeine-evoked $[Ca^{2+}]_i$ transient amplitude is greater than could be accounted for by a change to buffering. We are confident that a reduction of SR Ca^{2+} is a key contributor to the reduced $[Ca^{2+}]_i$ transient.

We next sought to explain the reduction in SR Ca^{2+} content. We observed an increase in NCX activity and a decrease in SERCA activity, which can account for the decreased SR Ca^{2+} levels in the presence of *S. nutans* (Eisner et al., 2017; Greensmith et al., 2014b; Reuter et al., 2005). A work by Bode *et al.* (Bode et al., 2011) demonstrates a relatively little dependence of SR Ca^{2+} levels on SERCA activity which – and given NCX activity continues to increase – may explain why SR Ca^{2+} content continues to fall during washout despite SERCA recovery. The progressive increase of NCX activity during washout may also account for the ultimate decrease of diastolic $[Ca^{2+}]_i$ (Blaustein and Lederer, 1999). This, however, appears to be a small effect and may be due to restored SERCA activity (Eisner et al., 2020).

In the presence of *S. nutans*, though the rate of systolic Ca^{2+} decay was decreased, only a modest (and non-significant) increase in cell relaxation time was observed. This, and a given

change of Ca^{2+} produced a smaller change of sarcomere length, suggests the drug may decrease myofilament sensitivity (Bers, 2002; Chung et al., 2016).

Chemical characterization

Fifty-one compounds were tentatively identified from the *S. nutans* using high-resolution orbitrap mass spectrometry and DAD detection: acetophenones, phenolic acids, amino acids, oxylipins, flavonoids, and coumarins.

Acetophenones and their glycoside derivatives are more abundant compounds in *S. nutans* (Loyola et al., 1984; Wang et al., 1999). Two metabolites, 4-hydroxy-3-(3-methyl-2-butenyl) acetophenone and 5-acetyl-6-hydroxy-2-isopropenyl-2,3-dihydro benzofurane, with relaxation activity on rat aorta, were isolated from *S. nutans* or *Xenophyllum poposum* V.A Funk (Fredi Cifuentes et al., 2018; Paredes et al., 2016).

The p-hydroxy acetophenone moiety is the most abundant backbone in various bioactive molecules from *S. nutans*. For example, isolated 4-hydroxy acetophenone from *Cynanchum wilfordii* (Maxim.) Hemsl. improves the vascular endothelial dysfunction involving the NO/cGMP pathway in rat aorta (Choi et al., 2012; Surcel et al., 2015). Furthermore, acetophenone derivatives could generate reactive oxygen species (ROS) and inhibit NADPH oxidase activity (Jaiswal and Kumar, 2022).

In addition, isopentenyl residue is also a very abundant backbone in bioactive molecules from *S. nutans* and would be involved in the vascular response. In rats, in endothelial cells of cerebral parenchymal arterioles and uterine radial arteries, the isopentenyl derivative produces a selective inhibition of Ca^{2+} influx by a Transient Receptor Potential Cation Channel (TRPV3) (Murphy et al., 2016; Pires et al., 2015).

In conclusion, *S. nutans* reduces the blood pressure in normotensive animals partially by decreasing of HR and cardiac contractility (inotropism). We present a cellular basis for this negative inotropy. Our results suggest that *S. nutans* increases NCX activity which decreases SR Ca^{2+} content leading to reduced systolic $[Ca^{2+}]_i$, thus contractility.

List of abbreviations:

ANOVA; Analysis of variance

Bpm; Beats per minute

HESI-II; Heated Electrospray Ionization

HR; Heart rate

K_{caff}; The rate constant of decay of the caffeine evoked $[Ca2^{+}]_i$ transient

k_{SERCA}; The rate constant of decay of the $[Ca^{2+}]_i$ transient in the sarcoendoplasmic reticulum Ca^{2+}-ATPase

k_{sys}; The rate constant of decay of the systolic Ca^{2+} transient

LC-MS; Liquid chromatography-mass spectrometry

LVP; Left ventricular pressure

m/z; Mass number of an ion by its charge number

MAP; Mean arterial pressure

MS; Mass spectrometry

NADPH; Nicotinamide Adenine Dinucleotide Phosphate Hydrogen

NCX; Sodium-calcium exchanger

NO/cGMP; nitric oxide / Cyclic guanosine monophosphate

PDA; Photodiode-Array Detection

RM ANOVA; Repeated measures analysis of variance

ROS; reactive oxygen species

SEM; Standard error of the mean

SERCA; Sarcoendoplasmic reticulum Ca^{2+}-ATPase

SR; Sarcoendoplasmic reticulum

TRPV3; Transient Receptor Potential Cation Channel

UHPLC-DAD-ESI-Q-OT-MS; Ultra-high-performance liquid-chromatography with diode array detection coupled with heated electrospray-ionization quadrupole-orbitrap mass spectrometric detection.

UHPLC-DAD-MS; Ultra-high-performance liquid-chromatography-diode array detector-tandem mass spectrometry

UV; Ultraviolet radiation

Contributions

Dr. Javier Palacios (clpalaci@unap.cl) participated in the design and performed some experiments and wrote the whole manuscript.

Dr. Adrian Paredes (adrian.paredes@uantof.cl), Dr. Fredi Cifuentes (fredi.cifuentes@uantof.cl) and Dr. Marcelo A Catalán (marcelo.catalan@uach.cl) participated in formal analysis, and drafting the manuscript.

Ángel Luis García-Villalón (angeluis.villalon@uam.es) performed the Langendorff experiments.

Dr. Jorge Bórquez (jorge.borquez@uantof.cl) and Dr. Mario J. Simirgiotis (mario.simirgiotis@gmail.com) performed the UHPLC-MS and drafting the manuscript.

Dr. Matthew Jones (M.A.Jones5@edu.salford.ac.uk), Amy Foster (A.Foster6@edu.salford.ac.uk) and David Greensmith (d.j.greensmith@salford.ac.uk) performed and analyzed the intracellular calcium experiments (fluorescence microscopy) and participated in the writing of the manuscript.

Conflict of interest

The authors declare no conflict of interest.

Supplementary Materials

The following are available online, UHPLC-DAD-ESI-Q-OT-MSn analysis, full mass spectra, and structure of several of the compounds identified by UHPLC-ESI-MSn from *S. nutans* hydroalcoholic extract.

Acknowledgments

We gratefully acknowledge Professor Andrew Trafford and Dr. Katherine Dibb (University of Manchester, UK) for providing the sheep cells used in our experiments.

Funding

Financial support by Fondecyt-Chile 1200610 to J.P.; Fondecyt-Chile 11190972 to A.P.; Fondecyt-Chile 1220075, and 1180059 to M.J.S. are gratefully acknowledged.

Legend figures

Figure 1. **Hypotensive effect of *S. nutans* in normotensive rats.** The results show the mean arterial pressure (MAP; **A**) and heart rate (**B**). The extract was administered intravenously, and the blood pressure in the carotid of anesthetized rats was measured. Values are mean ± standard error of the mean of 5 experiments. Statistically significant differences: $P < 0.01$ and $P < 0.001$ vs. basal.

Figure 2. **Effect of *S. nutans* on cardiac function of Langendorff isolated heart system.** The first protocol used an HR remained constant at 360 BMP (**A** and **B**). The second protocol allowed the heart to beat freely (**C** and **D**). Values are mean ± standard error of the mean of 5-3 experiments. Statistically significant differences: $P < 0.05$, $P < 0.01$ and $P < 0.001$ vs. basal.

Figure 3: The concentration-dependent effect of S. nutans on global $[Ca^{2+}]_i$ and contractility. (A) Mean $[Ca^{2+}]_i$ transient amplitude. (B) Mean systolic shortening. N= 25

Figure 4. The effects of *S. nutans* on global $[Ca^{2+}]_i$ in isolated sheep ventricular myocytes. (A) Specimen $[Ca^{2+}]_i$ transients from a cell field stimulated at 0.5 Hz. For each cell, 5 steady-state transients (indicated by square brackets) were averaged in control, *S. nutans* then washout (n = 24 cells). (B) Mean $[Ca^{2+}]_i$ transient amplitude. (C) Mean diastolic $[Ca^{2+}]_i$. (D) Specimen normalized Ca^{2+} transients to permit direct comparison of the rate of $[Ca^{2+}]_i$ decay. Dashed overlays represent single exponential decay fits. (E) Mean k_{sys}. Statistics indicators are placed above a bar compared to control.

Figure 5. The effects of *S. nutans* on contractility in isolated sheep ventricular myocytes. (A) Specimen contractility transients from a cell field stimulated at 0.5 Hz. For each cell, 5 steady-state transients (indicated by square brackets) were averaged in control, *S. nutans* then washout (n = 23 cells). (B) Mean systolic shortening. (C) Mean diastolic sarcomere length. (D) Mean relaxation time. (E) Phase plane analysis to determine the dependence of cell shortening on $[Ca^{2-}]_i$. The bars show the mean slope of the dependence of change of cell length on change of $[Ca^{2+}]_i$. Statistics indicators are placed above a bar compared to control.

Figure 6. The effects of *S. nutans* on SR Ca^{2+} content and the Ca^{2+} removal pathways. Relative changes to SR Ca^{2+} content were estimated by measuring the amplitude of caffeine

evoked $[Ca^{2+}]_i$ transients. Specimens are provided in (A). (B) Mean caffeine evoked $[Ca^{2+}]_i$ transient amplitude. (C) Mean k_{caff} (rate constant of decay of the caffeine-evoked Ca^{2+} transient). (D) Mean calculated k_{SERCA}. n = 13 for B and C and 11 for D. Statistics indicators placed above a bar compared to control.

Figure 7. UHPLC-MS chromatogram total ion current of hydroalcoholic extract of *S. nutans*. Total ion current (A), UV at 280 nm (B). The peak numbers correspond to those identified in **Supplementary Table S1.**

References

Bers, D.M., 2002. Cardiac excitation-contraction coupling. Nature. https://doi.org/10.1038/415198a

Blaustein, M.P., Lederer, W.J., 1999. Sodium/calcium exchange: Its physiological implications. Physiol Rev. https://doi.org/10.1152/physrev.1999.79.3.763

Bode, E.F., Briston, S.J., Overend, C.L., O'Neill, S.C., Trafford, A.W., Eisner, D.A., 2011. Changes of SERCA activity have only modest effects on sarcoplasmic reticulum Ca 2+ content in rat ventricular myocytes. Journal of Physiology 589. https://doi.org/10.1113/jphysiol.2011.211052

Choi, D.H., Lee, Y.J., Kim, J.S., Kang, D.G., Lee, H.S., 2012. Cynanchum wilfordii ameliorates hypertension and endothelial dysfunction in rats fed with high fat/cholesterol diets. Immunopharmacol Immunotoxicol 34. https://doi.org/10.3109/08923973.2011.569889

Chung, J.H., Biesiadecki, B.J., Ziolo, M.T., Davis, J.P., Janssen, P.M.L., 2016. Myofilament calcium sensitivity: Role in regulation of in vivo cardiac contraction and relaxation. Front Physiol. https://doi.org/10.3389/fphys.2016.00562

Cifuentes, F, Palacios, J., Kuzmicic, J., Carvajal, L., Muñoz, F., Quispe, C., Nwokocha, C.R., Morales, G., Norambuena-Soto, I., Chiong, M., Paredes, A., 2018. Vasodilator and hypotensive effects of pure compounds and hydroalcoholic extract of Xenophyllum poposum (Phil) V.A Funk (Compositae) on rats. Phytomedicine 50, 99–108. https://doi.org/10.1016/j.phymed.2018.09.226

Cifuentes, Fredi, Palacios, J., Kuzmicic, J., Carvajal, L., Muñoz, F., Quispe, C., Nwokocha, C.R., Morales, G., Norambuena-Soto, I., Chiong, M., Paredes, A., 2018. Vasodilator and hypotensive effects of pure compounds and hydroalcoholic extract of Xenophyllum poposum (Phil) V.A Funk (Compositae) on rats. Phytomedicine 50. https://doi.org/10.1016/j.phymed.2018.09.226

Cifuentes, Fredi, Paredes, A., Palacios, J., Muñoz, F., Carvajal, L., Nwokocha, C.R., Morales, G., 2016. Hypotensive and antihypertensive effects of a hydroalcoholic extract from Senecio nutans Sch. Bip. (Compositae) in mice: Chronotropic and negative inotropic effect, a nifedipine-like action. J Ethnopharmacol. https://doi.org/10.1016/j.jep.2015.12.048

Cifuentes, F, Paredes, A., Palacios, J., Muñoz, F., Carvajal, L., Nwokocha, C.R., Morales, G., 2016. Hypotensive and antihypertensive effects of a hydroalcoholic extract from Senecio nutans Sch. Bip. (Compositae) in mice: Chronotropic and negative inotropic effect, a nifedipine-like action. J Ethnopharmacol 179, 367–374. https://doi.org/10.1016/j.jep.2015.12.048

Dibb, K.M., Graham, H.K., Venetucci, L.A., Eisner, D.A., Trafford, A.W., 2007. Analysis of cellular calcium fluxes in cardiac muscle to understand calcium homeostasis in the heart. Cell Calcium 42. https://doi.org/10.1016/j.ceca.2007.04.002

Eisner, D.A., Caldwell, J.L., Kistamás, K., Trafford, A.W., 2017. Calcium and Excitation-Contraction Coupling in the Heart. Circ Res. https://doi.org/10.1161/CIRCRESAHA.117.310230

552 Eisner, D.A., Caldwell, J.L., Trafford, A.W., Hutchings, D.C., 2020. The Control of Diastolic Calcium in
553 the Heart: Basic Mechanisms and Functional Implications. Circ Res.
554 https://doi.org/10.1161/CIRCRESAHA.119.315891

555 Greensmith, D.J., 2014. Ca analysis: An excel based program for the analysis of intracellular
556 calcium transients including multiple, simultaneous regression analysis. Comput Methods
557 Programs Biomed 113. https://doi.org/10.1016/j.cmpb.2013.09.004

558 Greensmith, D.J., Galli, G.L.J., Trafford, A.W., Eisner, D.A., 2014a. Direct measurements of SR free
559 Ca reveal the mechanism underlying the transient effects of RyR potentiation under
560 physiological conditions. Cardiovasc Res 103. https://doi.org/10.1093/cvr/cvu158

561 Greensmith, D.J., Galli, G.L.J., Trafford, A.W., Eisner, D.A., 2014b. Direct measurements of SR free
562 Ca reveal the mechanism underlying the transient effects of RyR potentiation under
563 physiological conditions. Cardiovasc Res 103. https://doi.org/10.1093/cvr/cvu158

564 Jaiswal, G., Kumar, P., 2022. Neuroprotective role of apocynin against pentylenetetrazole kindling
565 epilepsy and associated comorbidities in mice by suppression of ROS/RNS. Behavioural Brain
566 Research 419. https://doi.org/10.1016/j.bbr.2021.113699

567 Khatib, R., Wilson, F., 2018. Pharmacology of Medications Used in the Treatment of
568 Atherosclerotic Cardiovascular Disease, in: Encyclopedia of Cardiovascular Research and
569 Medicine. https://doi.org/10.1016/b978-0-12-809657-4.99756-4

570 LaCombe, P., Lappin, S.L., 2020. Physiology, Afterload Reduction, StatPearls.

571 Loyola, L.A., Pedreros, S., Morales, G., 1985. Para-hydroxyacetophenone derivatives from Senecio-
572 Graveolens. Phytochemistry 24, 1600–1602. https://doi.org/10.1016/s0031-9422(00)81074-2

573 Murphy, T. v., Kanagarajah, A., Toemoe, S., Bertrand, P.P., Grayson, T.H., Britton, F.C., Leader, L.,
574 Senadheera, S., Sandow, S.L., 2016. TRPV3 expression and vasodilator function in isolated
575 uterine radial arteries from non-pregnant and pregnant rats. Vascul Pharmacol 83.
576 https://doi.org/10.1016/j.vph.2016.04.004

577 Paredes, A., Palacios, J., Quispe, C., Nwokocha, C.R., Morales, G., Kuzmicic, J., Cifuentes, F., 2016.
578 Hydroalcoholic extract and pure compounds from Senecio nutans Sch. Bip (Compositae)
579 induce vasodilation in rat aorta through endothelium-dependent and independent
580 mechanisms. J Ethnopharmacol 192. https://doi.org/10.1016/j.jep.2016.07.008

581 Pires, P.W., Sullivan, M.N., Pritchard, H.A.T., Robinson, J.J., Earley, S., 2015. Unitary TRPV3 channel
582 ca2+ influx events elicit endothelium-dependent dilation of cerebral parenchymal arterioles.
583 Am J Physiol Heart Circ Physiol 309. https://doi.org/10.1152/ajpheart.00140.2015

584 Reuter, H., Pott, C., Goldhaber, J.I., Henderson, S.A., Philipson, K.D., Schwinger, R.H.G., 2005. Na+-
585 Ca2+exchange in the regulation of cardiac excitation-contraction coupling. Cardiovasc Res.
586 https://doi.org/10.1016/j.cardiores.2005.04.031

587 Schotola, H., Sossalla, S.T., Renner, A., Gummert, J., Danner, B.C., Schott, P., Toischer, K., 2017. The
588 contractile adaption to preload depends on the amount of afterload. ESC Heart Fail 4.
589 https://doi.org/10.1002/ehf2.12164

590 Surcel, A., Ng, W.P., West-Foyle, H., Zhu, Q., Ren, Y., Avery, L.B., Krenc, A.K., Meyers, D.J., Rock,
591 R.S., Anders, R.A., Meyers, C.L.F., Robinson, D.N., 2015. Pharmacological activation of myosin
592 ii paralogs to correct cell mechanics defects. Proc Natl Acad Sci U S A 112.
593 https://doi.org/10.1073/pnas.1412592112

594 Trafford, A.W., Díaz, M.E., Eisner, D.A., 1999. A novel, rapid and reversible method to measure Ca
595 buffering and time- course of total sarcoplasmic reticulum Ca content in cardiac ventricular
596 myocytes. Pflugers Arch 437. https://doi.org/10.1007/s004240050808

597 Varro, A., Negretti, N., Hester, S.B., Eisner, D.A., 1993. An estimate of the calcium content of the
598 sarcoplasmic reticulum in rat ventricular myocytes. Pflugers Arch 423.
599 https://doi.org/10.1007/BF00374975

600 Villagrán, C., Romo, M., Castro, V., 2003. Etnobotánica del Sur de los Andes de la primera región de
601 Chile: Un enlace entre las culturas altiplánicas y las de quebradas altas del Loa superior.
602 Chungará (Arica) 35. https://doi.org/10.4067/s0717-73562003000100005

603

A Hydroalcoholic Extract of *Senecio nutans* SCh. Bip (Asteraceae); its effects on cardiac function and chemical characterization

Javier Palacios[a*], Adrián Paredes[b,c], Fredi Cifuentes[c,d], Marcelo A. Catalán[e], Angel Luis García-Villalón[f], Jorge Borquez[b], Mario J. Simirgiotis[g], Matthew Jones[h], Amy Foster[h], David J. Greensmith[h*]

[a] Laboratorio de Bioquímica Aplicada, Química y Farmacia, Facultad de Ciencias de la Salud, Universidad Arturo Prat, Iquique 1110939, Chile. clpalaci@unap.cl (J.P.)

[b] Departamento de Química, Facultad de Ciencias Básicas, Universidad de Antofagasta, Antofagasta 1271155, Chile. adrian.paredes@uantof.cl (A.P.), jorge.borquez@uantof.cl (J.B.)

[c] Instituto Antofagasta (IA), Universidad de Antofagasta, Antofagasta 1271155, Chile

[d] Departamento de Biomédico, Facultad Ciencias de la Salud, Universidad de Antofagasta, Antofagasta 1271155, Chile. fredi.cifuentes@uantof.cl (F.C.)

[e] Instituto de Fisiología, Facultad de Medicina, Universidad Austral de Chile, Valdivia 5090000, Chile. marcelo.catalan@uach.cl (M.A.C.)

[f] Departamento de Fisiología, Facultad de Medicina, Universidad Autónoma de Madrid, 28029 Madrid, Spain. angeluis.villalon@uam.es (A.L.GV.)

[g] Center for Interdisciplinary Studies on the Nervous System (CISNe), Universidad Austral de Chile, Valdivia, 5090000, Chile. simirgiotis@gmail.com (M.J.S.)

[h] Biomedical Research Centre, School of Science, Engineering and Environment, The University of Salford, Salford, United Kingdom. M.A.Jones9@salford.ac.uk (M.J.), A.Foster6@edu.salford.ac.uk (A.F.), d.j.greensmith@salford.ac.uk (D.J.G.)

[*]Corresponding author: clpalaci@unap.cl +56-57-2526910 (J.P.) and d.j.greensmith@salford.ac.uk +44 1612952170 (D.J.G.)

Abstract

Ethnopharmacology relevance; The plant *Senecio nutans* SCh. Bip. is used by Andean communities to treat altitude sickness. Recent evidence suggests it may produce vasodilation and negative cardiac inotropy, though the cellular mechanisms have not been elucidated.
Purpose: To determinate the mechanisms action of *S. nutans* on cardiovascular function in normotensive animals.
Methods: The effect of the extract on rat blood pressure was measured with a transducer in the carotid artery and intraventricular pressure by a Langendorff system. The effects on sheep ventricular intracellular calcium handling and contractility were evaluated using photometry. Ultra-high-performance liquid-chromatography with diode array detection coupled with heated electrospray-ionization quadrupole-orbitrap mass spectrometric detection (UHPLC-DAD-ESI-Q-OT-MSn) was used for extract chemical characterization.
Results: In normotensive rats, *S. nutans* (10 mg/Kg) reduced mean arterial pressure (MAP) by 40 % ($p < 0.05$), causing a dose-dependent coronary artery dilation and decreased left ventricular pressure. In isolated cells, *S. nutans* extract (1 µg/ml) rapidly reduced the $[Ca^{2+}]_i$ transient amplitude and sarcomere shorting by 40 and 49 % ($p<0.001$), respectively. The amplitude of the caffeine evoked $[Ca^{2+}]_i$ transient was reduced by 24 % ($p<0.001$), indicating reduced sarcoplasmic reticulum (SR) Ca^{2+} content. Sodium-calcium exchanger (NCX) activity increased by 17 % ($p<0.05$), while sarcoendoplasmic reticulum Ca^{2+}-ATPase (SERCA) activity was decreased by 21 % ($p<0.05$). LC-MS results showed the presence of vitamin C, malic acid, and several antioxidant phenolic acids reported for the first time. Dihydroeuparin and 4-hydroxy-3-(3-methylbut-2-enyl) acetophenone were abundant in the extract.
Conclusion: In normotensive animals, *S. nutans* partially reduces MAP by decreasing heart rate and cardiac contractility. This negative inotropy is accounted for by decreased SERCA activity and increased NCX activity which reduces SR Ca^{2+} content. These results highlight the plant's potential as a source of novel cardio-active phytopharmaceuticals or nutraceuticals.

Keywords: Cardiac function; contractility; endemic plants; intracellular calcium; mass spectrometry; myocyte.

Introduction

Senecio nutans (Sch.) Bip. (Synonyms: *Senecio graveolens* Wedd, *Senecio graveolens var. Psiloachaenius* Cabrera) is a perennial shrub approximately 20-60 cm high that grows in the Andes of Chile, Argentina, Perú, and Bolivia at 3500-5000 m.a.s.l. (Villagrán et al., 2003). It belongs to the family Asteraceae and a group of medicinal plants colloquially known as "Chachacoma".

Previous studies on this plant reported the presence of several exciting acetophenones (Loyola et al., 1985), which were bioactive compounds for altitude sickness and possessed cytotoxic activity (Cifuentes et al., 2016; Echiburú-Chau et al., 2014).

Our previous work revealed extracts of *S.nutans* exhibit hypotensive properties in normotensive rats and mice (Fredi Cifuentes et al., 2016). Here, extracts decreased heart rate (HR) and prolonged corrected QT (QTc). This bradycardia maybe due to reduced sino-atrial node activity as indicated by experiments using the isolated right atrium of normotensive rats (Fredi Cifuentes et al., 2016). Interestingly, the cardiovascular effect of *S. nutans* were similar to those displayed by Ca^{2+} channel blockers such as nifedipine, which decreases the frequency of beats of the right atrium and papillary muscle contractility of the left ventricle of. Furthermore, we demonstrated a direct negatively inotropic effect in intact hearts (Fredi Cifuentes et al., 2016), though the cellular basis of this phenomenon remains unknown.

In other work, we found *S. nutans* promotes vasodilation via Ca^{2+} and nitric oxide-dependent mechanisms (Paredes et al., 2016). Here, pre-incubation of intact aortic rings with *S. nutans* extracts reduced the contractile response to phenylephrine (PE) by blocking inward Ca^{2+} currents (Paredes et al., 2016).

Collectively, this evidence suggests *S. nutans* may be of value as a hypotensive agent. Despite this, an investigation of the cardiac cellular effects, or detailed metabolome analysis of the bioactive hydroalcoholic extract has yet to be reported. Therefore, the objective of the present study was to determine the mechanism of action of *S. nutans* on cardiovascular function in normotensive animals. We investigated (1) the hypotensive actions of *S. nutans in vivo*; (2) the cellular basis of the negative cardiac inotropy; and (3) the phytochemical fingerprint (UHPLC-DAD-ESI-Q-OT-MS) of *S. nutans*

Materials and Methods

Plant Material

S. nutans Sch. Bip was collected in the village of Toconce (22°15'11.16'' S, 68°5'44.68'' W, at 3,788 m.a.s.l.), North of Chile, Antofagasta Region. Dr. Roberto Rodríguez, Universidad de Concepción, Chile identified the plant (herbarium for collection; voucher # CONC 139.929).

Extraction preparation

The plant material (aerial parts) was ground and dried at room temperature. The powdered plant (2 Kg dry) was put into a cotton bag and immersed in 4 L of a mixture of EtOH: H_2O (1:1). After 72 h at room temperature, the solution was filtered (Whatman N^o 4) and concentrated on a rotary evaporator (50° C), and the result was a quarter of the initial volume. We repeated this method several times to obtain a final colorless solution. The lyophilized hydroalcoholic extract was stored at 4°C until use. The extraction yield was 19%.

Animals

Experiments on isolated hearts (Langendorff system) used male Sprague Dawley rats (6–8 weeks old; 170–200 g). The animals were randomized and housed at a room temperature of 22–25 °C in a light/dark photoperiod (12 hours each, lights were turned on at 8:00 am and turned off at 08:00 pm). The animal had *ad libitum* access to water and food (Champion, Santiago). Two groups of normotensive male rats were used in this study; group 1 (n = 5) for blood pressure protocol and group 2 for Langendorff protocol (n = 5). The animal research committee of Antofagasta University approved the experimental protocol (CEIC #275/2020). Experiments on cells used Welsh sheep by the Animals (Scientific Procedures) Act, UK, 1986, Directive 2010/63/EU of the European Parliament and local ethical review boards.

Blood pressure and heart rate measurements

As described in a previous study, MAP and HR were measured in rats (F Cifuentes et al., 2018). The rats were anesthetized with ketamine (42 mg/Kg, i.p.) and xylazine (5 mg/Kg, i.p.). We measured the blood pressure in the carotid artery and administered the extract (5, 10, 20, and 40 mg/Kg of body weight) through the saphenous vein. The doses of the extract were based on our previous study (Fredi Cifuentes et al., 2016). In that study, we found that 40 mg/Kg of body weight reduced the increase in blood pressure induced by angiotensin II. Therefore, doses below 40 mg/Kg were the focus of this physiological study.

Langendorff isolated the heart system

Briefly, animals were anesthetized, and the heart was quickly removed and mounted on the Langendorff system (constant flow of 10 mL/min of buffer). Krebs-Henseleit buffer (KHB) contains (in mM); 4.7 KCl, 1.2 KH_2PO_4, 118 NaCl, 25 Na_2HCO_3, 1.2 $MgSO_4$, 1.75 $CaCl_2$, 0.5 EDTA and 8 D-glucose (pH 7.4; 37°C; 95% O_2 and 5% CO_2). A ball of polyvinyl was inserted into the left ventricle and filled with 0.9% NaCl solution to measure contractile function. The heart was perfused with extract (1, 10, 100, 300, or 1000 μg/mL). The doses used in the extract for the Langendorff protocol were the same used in vascular reactivity experiments previously reported (Paredes et al., 2016). In this case, we found that 100 μg/mL extract caused a significant relaxation of rat aorta. The PoweLab8 system (ADInstruments, Australia) was used.

Intracellular Ca^{2+} and contractility measurements in isolated sheep ventricular myocytes.

Sheep ventricular myocytes were enzymatically isolated - by retrograde perfusion of the coronary arteries with collagenase and protease - as previously described (Greensmith et al., 2014a) and then loaded with the acetoxymethyl ester (AM) form of fura–2 (1 μM) for 10 min at room temperature. During Ca^{2+} measurements, cells were field stimulated at 0.5 Hz and perfused (37 °C) with a solution containing (in mM): NaCl 140, HEPES 10, glucose 10, KCl 4, probenecid 2, $MgCl_2$ 1, $CaCl_2$ 1.8, pH 7.35 with NaOH. The probenecid prevents loss of fura–2 from the cell at 37°C. Fura–2 was excited sequentially (200 Hz) at 340 and 380 nm using OptoLED light sources (Cairn Research, UK). Emitted fluorescence was measured via a 515 nm long-pass filter using a photomultiplier tube coupled to a photometry system (Cairn Research UK). Changes in cytoplasmic Ca^{2+} were inferred from the ratio of light emitted at

340:380 nm, calibrated using custom-written software (Greensmith, 2014). Cell contractility was evaluated simultaneously by measuring sarcomere length using a MyoCamS high-speed camera and SarcLen acquisition module (Ion Optix, USA).

Measurement of SR Ca^{2+} content and the activity of the Ca^{2+} removal mechanisms

Relative changes to Sarcoplasmic Reticulum (SR) Ca^{2+} content were measured by comparing the amplitude of Ca^{2+} transients evoked by applying 10 mM caffeine which causes rapid emptying of the SR. The descending phase of the systolic Ca^{2+} transient was fitted with a single exponential decay (Greensmith, 2014). Here, the rate constant of decay (k_{sys}) depends on the combined activity of the Sarco-Endoplasmic Reticulum Ca^{2+} ATPase (SERCA) and Sodium-Calcium Exchanger (NCX), whereas that of the caffeine evoked Ca^{2+} transient (k_{caff}) predominantly depends on NCX. Subtracting these rate constants gives k_{SERCA} and a calculated indication of SERCA activity.

UHPLC-DAD-ESI-Q-OT-MSn Instrument

Liquid chromatography (UHPLC-diode array- electrospray ionization- quadrupole orbitrap high-resolution-mass spectrometry) was performed as described in **Supplementary Information.**

Chemicals

Sephadex LH-20 was bough to Pharmacia Fine Chemicals (Piscataway, NJ, USA). While the following substances were obtained from Merck (Santiago, Chile); acetonitrile, methanol, hexane, and ethyl acetate.

Statistical Analysis

SEM (mean ± standard error of the mean) was used in this study. One-way ANOVA and one-way RM ANOVA were used to analyze statistically the data, followed by *post hoc* Bonferroni or Tukey tests. Graph Pad Prism, version 5.0. (GraphPad Software, Inc., La Jolla, CA, USA) and SigmaPlot version 12.0 (Systat Software Inc, USA) was used. A $p < 0.05$ was considered statistically different.

Results

The hydroalcoholic extract from S. nutans causes a hypotensive effect in rats.

We measured in vivo arterial blood pressure in anesthetized rats to determine whether our results may have clinical implications. MAP started to decrease at 10 mg/Kg of *S. nutans* extract: 130 ± 4 mmHg basal versus 75 ± 5 mmHg with 10 mg/Kg extract ($P< 0.01$; **Fig. 1A**). However, HR decreased at 40 mg/Kg extract (289 ± 7 bpm basal versus 231 ± 9 bpm with extract; $P < 0.01$; **Fig. 1B**).

S. nutans decrease the coronary pressure and the cardiac contractility in the Langendorff system.

The coronary and left ventricular pressure (LVP) were measured to gain insight into the extract's role in cardiac function. In the first Langendorff protocol, the cardiac contractility was determined while the heart rate was kept constant (360 bpm). *S. nutans* decreased the coronary pressure significantly ($P < 0.05$): 54 ± 6 mmHg basal versus 25 ± 11 mmHg with 100 μg/mL (**Fig. 2A**). While the LVP slightly decreased at the same extract concentration (75 ± 6 mmHg basal versus 44 ± 18 mmHg with 100 μg/mL), and it was abolished at 1000 μg/mL, **Fig. 2B**). After washing out, the LVP partially recovered (22 ± 13 mmHg). Since coronary and LV pressure did not completely recover during washout following exposure to 1000 μg/ml, we reduced the dose to 300 μg/ml.

In the second protocol, we allowed the heart to beat freely. Again, the coronary pressure decreased significantly in dose-dependent way, 67 ± 1 mmHg basal versus 62 ± 1 mmHg at 10 μg/mL ($P<0.05$), 60 ± 1 mmHg at 100 μg/mL ($P< 0.01$), and 50 ± 2 mmHg at 300 μg/mL ($P<0.001$) (**Fig. 2C**). In this protocol, the HR increased (192 ± 5 bpm basal versus 215 ± 6 bpm with 300 μg/mL) when coronary pressure decreased, but statistical analysis did not show significance (**Fig. 2D**). Here, we did not observe a reduction in LVP at all (data not shown).

The effects of S. nutans on cardiac intracellular Ca^{2+} and contractility dynamics in isolated cardiac myocytes

To evaluate whether changes to cell function contribute to the effects observed in isolated hearts, we next measured the effect on intracellular calcium ($[Ca^{2+}]_i$) and contractility dynamics on isolated cardiac myocytes. The sheep was chosen as the study model as (1) they are particularly convenient for the photometric methods used in this study, (2) for alignment

to 3Rs principles and (3) because the fundamental cardiac cellular physiology of sheep is similar to that of rat. *S. nutans* extracts (0.01, 0.1, 1, 10 and 100 µg/ml) produced a concentration-dependent decrease in both the Ca^{2+} transient amplitude and systolic shortening (**Fig. 3**). A 1 µg/ml concentration was used for all subsequent detailed analyses.

The experiment represented in **Fig. 4A** and **D** (representative of data from 24 cells) shows that application of 1 µg / ml S. *nutans extract* rapidly (10-20 s) decreased the amplitude and rate of decay of the $[Ca^{2+}]_i$ transient to a lower steady state. On average, systolic Ca^{2+} (**Fig. 4B**) was reduced by 40 ± 4 % ($p < 0.001$) which partially reversed to 69 ± 8 % ($p = 0.02$) of control upon washout. Diastolic $[Ca^{2+}]_i$ (**Fig. 4C**) progressively decreased during the experiment to 93 ± 3 % ($p = 0.04$) of control by the end of washout. The rate constant of systolic Ca^{2+} decay (k_{sys}, **Fig 4E**) was reduced by 17 ± 4 % ($p = 0.002$), which reversed to levels equivalent to control on washout.

The experiment represented in **Fig. 5A** shows the associated effect on cell contractility. On average, systolic sarcomere shortening (**Fig 5B**) was reduced by 49 ± 4 % ($p < 0.001$). Diastolic sarcomere length (**Fig 5C**) was unaltered, and while an increase in relaxation rate (**Fig 5D**) was apparent, this did not reach significance. To determine the dependence of sarcomere length on $[Ca^{2+}]_i$, phase plane analysis was performed. **Fig. 5E** shows that the slope of sarcomere length versus $[Ca^{2+}]_i$ was reduced by 28 ± 8 % ($p = 0.02$) and then reversed on washout.

The effects of S. nutans on SR Ca^{2+} content and systolic Ca^{2+} removal pathways

The experiment represented in **Fig. 6A** (representative of data from 13 cells) shows that application of 1 µg / ml S. *nutans extracts* decreased the amplitude of caffeine-evoked $[Ca^{2+}]_i$ transients indicating a relative decrease in SR Ca^{2+} content. On average, relative SR Ca^{2+} content (**Fig 6B**) was decreased by 24 ± 4 % ($p < 0.001$) which progressed to 41 ± 6 % ($p < 0.001$) during washout. The rate of Ca^{2+} removal was determined to understand the cause of the decrease of SR Ca^{2+} content. The rate constant of decay of the caffeine induced $[Ca^{2+}]_i$ transient (k_{caff}) (**Fig. 6C**) was increased by 17 ± 4 % ($p = 0.04$), progressing to 41 ± 7 % ($p < 0.001$) during washout and indicating associated increases of NCX activity. The SERCA activity was calculated as $k_{SERCA} = k_{sys} - k_{caff}$ and was decreased by 21 ± 8 % ($p = 0.02$) and then reversed on washout (**Fig. 6D**).

High-Resolution UHPLC-DAD-ESI-Q-Orbitrap-Mass Spectrometry Analysis

The analysis of the phenolic composition of *S. nutans* was carried out by UHPLC-DAD-ESI-Q-OT-MS using four detection channels (330, 280, 254, and 440 nm, plus 3D DAD plotting) and the negative heated ionization mode (HESI-II). The total ion current and Photodiode-Array Detection (PDA) chromatograms of the hydroalcoholic extract are shown in **Fig. 7**.

Firstly, the phenolic compounds were identified by the analysis of each ultraviolet (UV) spectra. Involves the determination of the molecular weight of each molecule and the analysis of the daughter ions (MS^n) detected for each parent molecule. The most intense peak corresponds to the deprotonated molecular ion $[M-H]^-$, followed by some $[2M-H]^-$ diagnostic adducts ions and some MS^n daughter ions in the negative ionization mode (HESI-II^-) MS^1 spectrum. The MS^n profiles of the detected molecules are shown in **Table S1 and Fig. S1,** and the characterization of the compounds follows below. In **Supplementary Fig. S2**, the tentative derivatives detected in *S. nutans* extract.

Simple organic acids

Peaks 2, 3, and 4 with molecular anions at m/z: 191.05611, 133.01425, 191.01973 were identified as quinic, malic, and citric acids ($C_7H_{11}O_6^-$, $C_4H_5O_5^-$ and $C_6H_7O_7^-$) (Brito et al., 2014; Echiburu-Chau et al., 2017), respectively.

Aminoacids

In positive mode, several underivatized amino acids were detected in *S. nutans* extract using the quadrupole-orbitrap analyzer (Le et al., 2014; Nemkov et al., 2015). Peak 1 with a molecular cation at m/z: 147.07695 was identified as glutamine ($C_5H_{11}O_3N_2^+$) and peak 6 as leucine or isoleucine ($C_6H_{14}O_2N^+$), Peak 10 as phenylalanine ($C_9H_{12}O_2N^+$) and peak 13 as asparagine ($C_4H_9O_3N_2^+$). Similarly, peak 16 with molecular cation at m/z: 205.09784 was identified as tryptophan ($C_{11}H_{13}O_2N_2^+$).

Acetophenones and related compounds

Peak 7 with an ion [M-H]- at m/z: 329.08795 was regarded as the glycoside 3,4-dihydroxyacetophenone 5-O-glucoside, ($C_{14}H_{17}O_9^-$), Peak 28 with an ion $[M-H]^-$ at *m/z*: 413.18198 as the *glycosyl* derivative: 3-methoxy-4-hydroxy-5-(3-methyl-2-butyl)

acetophenone 2-O-glucoside ($C_{20}H_{29}O_9^-$). In the same manner, peak 26 with an ion $[M-H]^-$ at *m/z*: 381.15561 was identified as 2-O-glucosyl-4-hydroxy-5-(3-methyl-2-butenyl) acetophenone ($C_{19}H_{25}O_8^-$), peak 27 with an ion $[M-H]^-$ at *m/z*: 411.16626 was tentatively characterized as another glycosyl derivative: 3-methoxy-4-hydroxy-5-(3-methyl-2-butenyl) acetophenone, 2-O-glucoside ($C_{20}H_{27}O_9^-$), peak 28 as 2-O-glucosyl-3-methoxy-4-hydroxy-5-(3-methyl-2-butyl) acetophenone ($C_{20}H_{29}O_9^-$) peak 32 was assigned to the reduced benzofurane and UV ray absorbent-sunscreen molecule dihydroeuparin (*m/z*: 217.08676, $C_{13}H_{13}O_3^-$) (Ortega et al., 2000; Tang et al., 1987), while peak 38 with a pseudo-molecular ion at *m/z*: 219.10242 as 2,4-dihydroxy-5-(3-methyl-2-butenyl) acetophenone ($C_{13}H_{15}O_3^-$). In the same manner, peak 37 (parent ion at *m/z*: 221.11983) was identified as the isomer of the later, 4-hydroxy-3-(1-en-3-methyl-3-butanol) acetophenone ($C_{13}H_{15}O_3^-$), Peak 40 with a parent ion at *m/z*: 249.11327 was identified as 5-acetyl-2,3-dihydro-6-hydroxy-7-methoxy-2-(isopropenyl)benzofurane ($C_{14}H_{17}O_4^+$) peak 4<2 with a pseudomolecular ion at *m/z*: 237.11334 was characterized as 5-acetyl-2,3-dihydro-6-hydroxy-2-(1-methyl-1-hydroxyetane)benzofurane ($C_{13}H_{17}O_4^+$). Finally, peak 31 with an ion $[M-H]^-$ at *m/z*: 203.10744 was identified as 4-hydroxy-3-(3-methyl-2-butenyl) acetophenone ($C_{13}H_{15}O_2^-$) and peak 47 as the non-substituted core structure acetophenone ($C_8H_9O^+$).

Phenolic acids

Several compounds were detected mainly in negative mode as phenolic acids. Peak 12 with an ion $[M-H]^-$ at *m/z*: 343.10361 was labeled as dehydro-caffeoyl-beta-D-glucopyranoside ($C_{15}H_{19}O_9^-$); these compounds have many bioactive effects, including acetylcholinesterase inhibition (Wang et al., 2017) and inhibition of the development of platelet aggregation and amplification of platelet activation (Fu et al., 2017), while peak 14 with an ion $[M-H]^-$ at *m/z*: 341.08795 was tentatively labeled as caffeoyl-beta-D-glucopyranoside ($C_{15}H_{17}O_9^-$). Accordingly, peak 19 with an ion $[M-H]^-$ at *m/z*: 383.09860 was identified as an acetylated caffeoyl-beta-D-glucopyranoside ($C_{17}H_{19}O_{10}^-$), while peak 24 with a pseudo-molecular ion at *m/z*: 367.10364 was regarded as 5-O-feruloylquinic acid ($C_{17}H_{19}O_9^-$), which was reported active against yeast glucosidase (Chen et al., 2014), peak 34 as *p*-coumaric acid ($C_9H_7O_3^-$), peak 25 with a molecular anion at *m/z*: 179.03471 was identified as caffeic acid ($C_9H_7O_3^-$), peaks 17 with pseudo-molecular ions at *m/z*: 515.11959 and daughter caffeoyl quinic ion at *m/z*: 353.08781 was identified as one of the isomers of dicaffeoylquinic acid ($C_{25}H_{23}O_{12}^-$),

peak 35 as chlorogenic acid, (*m/z*: 353.08798) peak 39 as 3-methyl-4-methoxycinnamic acid ($C_{11}H_{11}O_3^-$), peak 34 as coumaric acid ($C_9H_7O_3^-$) and peak 36 as cinnamic acid (*m/z*: 147.04454, $C_9H_7O_2^-$). These caffeoyl and feruloyl quinic acid derivatives have displayed previously anti-diabetic activity (Chen et al., 2014).

Oxylipins

Fatty acid components of healthy food such as asparagus are known as oxylipins; these important dietary compounds possess high antioxidant activity (Jiménez-Sánchez et al., 2016) and some antifungal activity (Martin-Arjol et al., 2010). Accordingly, peak 18 was identified as a glycosyl fatty acid conjugate, tetrahydroxydodecaenoic acid-O-glucoside ($C_{18}H_{31}O_{12}^-$). In the same manner, peak 5 was characterized in positive mode as the amino fatty acid derivative amineoxodecanoic acid ($C_{10}H_{20}O_3N^+$) (Kuno et al., 2015), peak 8 with a pseudomolecular cation at *m/z*: 174.14940 as amine-nonanoic acid ($C_9H_{20}O_2N^+$) and peak 9 with molecular cation at *m/z*: 160.13373 as aminoctanoic acid ($C_8H_{18}O_2N^+$). Peak 11 was assigned as the saturated small 8 carbons fatty acid caprylic acid ($C_8H_{17}O_2^+$). Finally, peaks 41 with an ion $[M-H]^-$ at *m/z*: 327.21793 was identified as trihydroxyoctadecadienoic acid ($C_{18}H_{31}O_5^-$) (Martin-Arjol et al., 2010) and peak 44 with 2 more hydrogens and an ion $[M-H]^-$ at *m/z*: 329.23346 as trihydroxyoctadecaenoic acid ($C_{18}H_{33}O_5^-$).

Flavonoids

Some compounds were characterized as quercetin or myricetin derivatives, peaks 43 and 51 (λ max: 254 and 354 nm) with molecular anions at *m/z*: 345.06171 and 343.08258 were characterized as: 3', 7-dimethoxymyricetin (Echiburu-Chau et al., 2017) and 7,4', 5'-trimethoxyquercetin, ($C_{17}H_{13}O_8^-$ and $C_{18}H_{15}O_7^-$), respectively. Peak 15 with an ion $[M-H]^-$ at *m/z*: 493.09885 was identified as a flavonol glycoside derivative: 7-methoxymyricetin 3-O-glucoside ($C_{22}H_{21}O_{13}^-$) and peak 29 with an ion $[M-H]^-$ at *m/z*: 549.12488 as its acetylated derivative: 7-acetyl-3-O-glucoside-3',4'-dimethoxymyricetin ($C_{25}H_{25}O_{14}^-$) while peak 22 with a ion $[M-H]^-$ at *m/z*: 491.11966 was characterized as 7,3'-dimethoxyquercetin 3-O-glucose ($C_{23}H_{23}O_{12}^-$). Peak 21 with a ion $[M-H]^-$ at *m/z*: 579.14819 was identified in positive mode as 5,6,7,4' -tetrahydroxyflavone-7-O-cynammoyl-glucose ($C_{30}H_{27}O_{12}^+$) and peak 20 as 5,6,7,4'-tetrahydroxyflavone-7-O-coumaroyl-glucose ($C_{30}H_{27}O_{13}^+$), while peak 23 with an ion $[M-H]^-$ at *m/z*: 507.11447 as: 3-O-glucosyl-3',4'-dimethoxymyricetin ($C_{23}H_{23}O_{13}^-$).

Coumarins

Peaks 45, 46, 48-50 were identified as coumarins (Simirgiotis et al., 2013b). The simple coumarin compound peak 45 was detected in positive mode (ion at *m/z*: 147.04446, $C_9H_7O_2^+$), while peak 49 was determined as umbelliferone ($C_9H_7O_3^+$) and peak 50 as scopoletin ($C_{10}H_9O_4^+$). Peak 30 with a pseudomolecular ion at *m/z*: 209.04518 was characterized as 8-hydroxyescopoletin or aesculetin ($C_{10}H_9O_5^+$) (Simirgiotis et al., 2013b), peak 33 as hydroxy-3-(1-en-3-methyl-3-butanol) acetophenone, peak 48 as herniatin ($C_{10}H_9O_3^+$) and peak 46 as 8-hydroxy-7-methoxy-scopoletin ($C_{11}H_{11}O_5^+$) (Echiburu-Chau et al., 2017) and peak 47 as acetophenone.

Discussion

This study, for the first time, showed the hypotensive properties of the hydroalcoholic extract of *Senecio nutans* are related to altered $[Ca^{2+}]_i$ handling and contractility in isolated cardiac myocytes.

Effect of S. nutans on blood pressure and isolated heart Langendorff

The extract was administered to anesthetic normotensive rats to assess whether *S. nutans* may have clinical consequences. The reduction in MAP would cause a decrease in HR and cardiac contractility. In a previous study, we demonstrated that oral extract administration for ten days in rats or intravenous administration in mice reduced the MAP (Fredi Cifuentes et al., 2016).

Notably, our results show that *S. nutans* caused coronary artery dilation in a dose-dependent way under both protocols; when the HR held constant at 360 bpm, or the heart was allowed to beat freely. The negative inotropic effect of *S. nutans* could explain by a lower peripheral vascular resistance. This hypothesis is supported because the extract caused coronary vasodilation, leading to a reduction in afterload (peripheral vascular resistance; (Khatib and Wilson, 2018) and an increase of the heart to preload as a function of afterload (Schotola et al., 2017).

In the second Langendorff protocol – where the heart was allowed to beat freely - an increase in the HR was observed while the coronary arteries dilated in the presence of *S. nutans*. Since the left ventricular pressure did not decrease (data not shown), we assume that the contractility of the heart did not change either. Therefore, it is possible that increased HR counteracted the effect of coronary artery dilatation on the decrease in afterload and blood pressure (LaCombe and Lappin, 2020).

This study showed a slight decrease of inotropic at submaximal doses of extract and significant reduction with maximal doses. However, in a previous study, we clarified that extract a significantly decreased ventricular contractility at submaximal doses in rat (F Cifuentes et al., 2016).

The effects of S. nutans on intracellular Ca^{2+} handling and contractility

To provide a cellular basis for the ventricular negative inotropy observed in the current and our previous study (F Cifuentes et al., 2016), we evaluated the effect of the extract on $[Ca^{2+}]_i$ and contractility in isolated myocytes. *S. nutans* decreases the $[Ca^{2+}]_i$ transient amplitude, accounting for reduced systolic shortening (Bers, 2002). The amplitude of the $[Ca^{2+}]_i$ transient is proportional to the third power of the SR Ca^{2+} content (Dibb et al., 2007). *S. nutans* reduced SR Ca^{2+} content to 76 % of control. This would be expected to decrease the $[Ca^{2+}]_i$ transient to $(0.76)^3 = 44$ %. The Ca^{2+} transient only decreased to 60 %, indicating that the decreased SR Ca^{2+} is more than enough to account for the $[Ca^{2+}]_i$ transient amplitude. We acknowledge, however, that we do not know if extracts of *S. nutans* alter Ca^{2+} buffering; thus, the relationship between total SR Ca^{2+} release and free Ca^{2+} (to which fura–2 fluorescence is proportional), so it is not possible to quantify the absolute change of SR Ca^{2+} content (Trafford et al., 1999; Varro et al., 1993). Indeed, this may explain why SR Ca^{2+} content progressively decreases during washout while the $[Ca^{2+}]_i$ partially recovers. Nonetheless, the *relative* change of caffeine-evoked $[Ca^{2+}]_i$ transient amplitude is greater than could be accounted for by a change to buffering. We are confident that a reduction of SR Ca^{2+} is a key contributor to the reduced $[Ca^{2+}]_i$ transient.

We next sought to explain the reduction in SR Ca^{2+} content. We observed an increase in NCX activity and a decrease in SERCA activity, which can account for the decreased SR Ca^{2+} levels in the presence of *S. nutans* (Eisner et al., 2017; Greensmith et al., 2014b; Reuter et al., 2005). A work by Bode *et al.* (Bode et al., 2011) demonstrates a relatively little dependence of SR Ca^{2+} levels on SERCA activity which – and given NCX activity continues to increase – may explain why SR Ca^{2+} content continues to fall during washout despite SERCA recovery. The progressive increase of NCX activity during washout may also account for the ultimate decrease of diastolic $[Ca^{2+}]_i$ (Blaustein and Lederer, 1999). This, however, appears to be a small effect and may be due to restored SERCA activity (Eisner et al., 2020).

In the presence of *S. nutans*, though the rate of systolic Ca^{2+} decay was decreased, only a modest (and non-significant) increase in cell relaxation time was observed. This, and a given

change of Ca^{2+} produced a smaller change of sarcomere length, suggests the drug may decrease myofilament sensitivity (Bers, 2002; Chung et al., 2016).

Chemical characterization

Fifty-one compounds were tentatively identified from the *S. nutans* using high-resolution orbitrap mass spectrometry and DAD detection: acetophenones, phenolic acids, amino acids, oxylipins, flavonoids, and coumarins.

Acetophenones and their glycoside derivatives are more abundant compounds in *S. nutans* (Loyola et al., 1984; Wang et al., 1999). Two metabolites, 4-hydroxy-3-(3-methyl-2-butenyl) acetophenone and 5-acetyl-6-hydroxy-2-isopropenyl-2,3-dihydro benzofurane, with relaxation activity on rat aorta, were isolated from *S. nutans* or *Xenophyllum poposum* V.A Funk (Fredi Cifuentes et al., 2018; Paredes et al., 2016).

The p-hydroxy acetophenone moiety is the most abundant backbone in various bioactive molecules from *S. nutans*. For example, isolated 4-hydroxy acetophenone from *Cynanchum wilfordii* (Maxim.) Hemsl. improves the vascular endothelial dysfunction involving the NO/cGMP pathway in rat aorta (Choi et al., 2012; Surcel et al., 2015). Furthermore, acetophenone derivatives could generate reactive oxygen species (ROS) and inhibit NADPH oxidase activity (Jaiswal and Kumar, 2022).

In addition, isopentenyl residue is also a very abundant backbone in bioactive molecules from *S. nutans* and would be involved in the vascular response. In rats, in endothelial cells of cerebral parenchymal arterioles and uterine radial arteries, the isopentenyl derivative produces a selective inhibition of Ca^{2+} influx by a Transient Receptor Potential Cation Channel (TRPV3) (Murphy et al., 2016; Pires et al., 2015).

In conclusion, *S. nutans* reduces the blood pressure in normotensive animals partially by decreasing of HR and cardiac contractility (inotropism). We present a cellular basis for this negative inotropy. Our results suggest that *S. nutans* increases NCX activity which decreases SR Ca^{2+} content leading to reduced systolic $[Ca^{2+}]_i$, thus contractility.

List of abbreviations:

ANOVA; Analysis of variance

Bpm; Beats per minute

HESI-II; Heated Electrospray Ionization

HR; Heart rate

K_{caff}; The rate constant of decay of the caffeine evoked $[Ca2^{+}]_i$ transient

k_{SERCA}; The rate constant of decay of the $[Ca^{2+}]_i$ transient in the sarcoendoplasmic reticulum Ca^{2+}-ATPase

k_{sys}; The rate constant of decay of the systolic Ca^{2+} transient

LC-MS; Liquid chromatography-mass spectrometry

LVP; Left ventricular pressure

m/z; Mass number of an ion by its charge number

MAP; Mean arterial pressure

MS; Mass spectrometry

NADPH; Nicotinamide Adenine Dinucleotide Phosphate Hydrogen

NCX; Sodium-calcium exchanger

NO/cGMP; nitric oxide / Cyclic guanosine monophosphate

PDA; Photodiode-Array Detection

RM ANOVA; Repeated measures analysis of variance

ROS; reactive oxygen species

SEM; Standard error of the mean

SERCA; Sarcoendoplasmic reticulum Ca^{2+}-ATPase

SR; Sarcoendoplasmic reticulum

TRPV3; Transient Receptor Potential Cation Channel

UHPLC-DAD-ESI-Q-OT-MS; Ultra-high-performance liquid-chromatography with diode array detection coupled with heated electrospray-ionization quadrupole-orbitrap mass spectrometric detection.

UHPLC-DAD-MS; Ultra-high-performance liquid-chromatography-diode array detector-tandem mass spectrometry

UV; Ultraviolet radiation

Contributions

Dr. Javier Palacios (clpalaci@unap.cl) participated in the design and performed some experiments and wrote the whole manuscript.

Dr. Adrian Paredes (adrian.paredes@uantof.cl), Dr. Fredi Cifuentes (fredi.cifuentes@uantof.cl) and Dr. Marcelo A Catalán (marcelo.catalan@uach.cl) participated in formal analysis, and drafting the manuscript.

Ángel Luis García-Villalón (angeluis.villalon@uam.es) performed the Langendorff experiments.

Dr. Jorge Bórquez (jorge.borquez@uantof.cl) and Dr. Mario J. Simirgiotis (mario.simirgiotis@gmail.com) performed the UHPLC-MS and drafting the manuscript.

Dr. Matthew Jones (M.A.Jones5@edu.salford.ac.uk), Amy Foster (A.Foster6@edu.salford.ac.uk) and David Greensmith (d.j.greensmith@salford.ac.uk) performed and analyzed the intracellular calcium experiments (fluorescence microscopy) and participated in the writing of the manuscript.

Conflict of interest

The authors declare no conflict of interest.

Supplementary Materials

The following are available online, UHPLC-DAD-ESI-Q-OT-MSn analysis, full mass spectra, and structure of several of the compounds identified by UHPLC-ESI-MSn from *S. nutans* hydroalcoholic extract.

Acknowledgments

We gratefully acknowledge Professor Andrew Trafford and Dr. Katherine Dibb (University of Manchester, UK) for providing the sheep cells used in our experiments.

Funding

Financial support by Fondecyt-Chile 1200610 to J.P.; Fondecyt-Chile 11190972 to A.P.; Fondecyt-Chile 1220075, and 1180059 to M.J.S. are gratefully acknowledged.

Legend figures

Figure 1. **Hypotensive effect of *S. nutans* in normotensive rats.** The results show the mean arterial pressure (MAP; **A**) and heart rate (**B**). The extract was administered intravenously, and the blood pressure in the carotid of anesthetized rats was measured. Values are mean ± standard error of the mean of 5 experiments. Statistically significant differences: $P < 0.01$ and $P < 0.001$ vs. basal.

Figure 2. **Effect of *S. nutans* on cardiac function of Langendorff isolated heart system.** The first protocol used an HR remained constant at 360 BMP (**A** and **B**). The second protocol allowed the heart to beat freely (**C** and **D**). Values are mean ± standard error of the mean of 5-3 experiments. Statistically significant differences: $P < 0.05$, $P < 0.01$ and $P < 0.001$ vs. basal.

Figure 3: The concentration-dependent effect of S. nutans on global $[Ca^{2+}]_i$ and contractility. (A) Mean $[Ca^{2+}]_i$ transient amplitude. (B) Mean systolic shortening. N= 25

Figure 4. The effects of *S. nutans* on global $[Ca^{2+}]_i$ in isolated sheep ventricular myocytes. (A) Specimen $[Ca^{2+}]_i$ transients from a cell field stimulated at 0.5 Hz. For each cell, 5 steady-state transients (indicated by square brackets) were averaged in control, *S. nutans* then washout (n = 24 cells). (B) Mean $[Ca^{2+}]_i$ transient amplitude. (C) Mean diastolic $[Ca^{2+}]_i$. (D) Specimen normalized Ca^{2+} transients to permit direct comparison of the rate of $[Ca^{2+}]_i$ decay. Dashed overlays represent single exponential decay fits. (E) Mean k_{sys}. Statistics indicators are placed above a bar compared to control.

Figure 5. The effects of *S. nutans* on contractility in isolated sheep ventricular myocytes. (A) Specimen contractility transients from a cell field stimulated at 0.5 Hz. For each cell, 5 steady-state transients (indicated by square brackets) were averaged in control, *S. nutans* then washout (n = 23 cells). (B) Mean systolic shortening. (C) Mean diastolic sarcomere length. (D) Mean relaxation time. (E) Phase plane analysis to determine the dependence of cell shortening on $[Ca^{2-}]_i$. The bars show the mean slope of the dependence of change of cell length on change of $[Ca^{2+}]_i$. Statistics indicators are placed above a bar compared to control.

Figure 6. The effects of *S. nutans* on SR Ca^{2+} content and the Ca^{2+} removal pathways. Relative changes to SR Ca^{2+} content were estimated by measuring the amplitude of caffeine

evoked $[Ca^{2+}]_i$ transients. Specimens are provided in (A). (B) Mean caffeine evoked $[Ca^{2+}]_i$ transient amplitude. (C) Mean k_{caff} (rate constant of decay of the caffeine-evoked Ca^{2+} transient). (D) Mean calculated k_{SERCA}. n = 13 for B and C and 11 for D. Statistics indicators placed above a bar compared to control.

Figure 7. UHPLC-MS chromatogram total ion current of hydroalcoholic extract of *S. nutans*. Total ion current (A), UV at 280 nm (B). The peak numbers correspond to those identified in **Supplementary Table S1.**

References

Bers, D.M., 2002. Cardiac excitation-contraction coupling. Nature. https://doi.org/10.1038/415198a

Blaustein, M.P., Lederer, W.J., 1999. Sodium/calcium exchange: Its physiological implications. Physiol Rev. https://doi.org/10.1152/physrev.1999.79.3.763

Bode, E.F., Briston, S.J., Overend, C.L., O'Neill, S.C., Trafford, A.W., Eisner, D.A., 2011. Changes of SERCA activity have only modest effects on sarcoplasmic reticulum Ca 2+ content in rat ventricular myocytes. Journal of Physiology 589. https://doi.org/10.1113/jphysiol.2011.211052

Choi, D.H., Lee, Y.J., Kim, J.S., Kang, D.G., Lee, H.S., 2012. Cynanchum wilfordii ameliorates hypertension and endothelial dysfunction in rats fed with high fat/cholesterol diets. Immunopharmacol Immunotoxicol 34. https://doi.org/10.3109/08923973.2011.569889

Chung, J.H., Biesiadecki, B.J., Ziolo, M.T., Davis, J.P., Janssen, P.M.L., 2016. Myofilament calcium sensitivity: Role in regulation of in vivo cardiac contraction and relaxation. Front Physiol. https://doi.org/10.3389/fphys.2016.00562

Cifuentes, F, Palacios, J., Kuzmicic, J., Carvajal, L., Muñoz, F., Quispe, C., Nwokocha, C.R., Morales, G., Norambuena-Soto, I., Chiong, M., Paredes, A., 2018. Vasodilator and hypotensive effects of pure compounds and hydroalcoholic extract of Xenophyllum poposum (Phil) V.A Funk (Compositae) on rats. Phytomedicine 50, 99–108. https://doi.org/10.1016/j.phymed.2018.09.226

Cifuentes, Fredi, Palacios, J., Kuzmicic, J., Carvajal, L., Muñoz, F., Quispe, C., Nwokocha, C.R., Morales, G., Norambuena-Soto, I., Chiong, M., Paredes, A., 2018. Vasodilator and hypotensive effects of pure compounds and hydroalcoholic extract of Xenophyllum poposum (Phil) V.A Funk (Compositae) on rats. Phytomedicine 50. https://doi.org/10.1016/j.phymed.2018.09.226

Cifuentes, Fredi, Paredes, A., Palacios, J., Muñoz, F., Carvajal, L., Nwokocha, C.R., Morales, G., 2016. Hypotensive and antihypertensive effects of a hydroalcoholic extract from Senecio nutans Sch. Bip. (Compositae) in mice: Chronotropic and negative inotropic effect, a nifedipine-like action. J Ethnopharmacol. https://doi.org/10.1016/j.jep.2015.12.048

Cifuentes, F, Paredes, A., Palacios, J., Muñoz, F., Carvajal, L., Nwokocha, C.R., Morales, G., 2016. Hypotensive and antihypertensive effects of a hydroalcoholic extract from Senecio nutans Sch. Bip. (Compositae) in mice: Chronotropic and negative inotropic effect, a nifedipine-like action. J Ethnopharmacol 179, 367–374. https://doi.org/10.1016/j.jep.2015.12.048

Dibb, K.M., Graham, H.K., Venetucci, L.A., Eisner, D.A., Trafford, A.W., 2007. Analysis of cellular calcium fluxes in cardiac muscle to understand calcium homeostasis in the heart. Cell Calcium 42. https://doi.org/10.1016/j.ceca.2007.04.002

Eisner, D.A., Caldwell, J.L., Kistamás, K., Trafford, A.W., 2017. Calcium and Excitation-Contraction Coupling in the Heart. Circ Res. https://doi.org/10.1161/CIRCRESAHA.117.310230

552 Eisner, D.A., Caldwell, J.L., Trafford, A.W., Hutchings, D.C., 2020. The Control of Diastolic Calcium in
553 the Heart: Basic Mechanisms and Functional Implications. Circ Res.
554 https://doi.org/10.1161/CIRCRESAHA.119.315891

555 Greensmith, D.J., 2014. Ca analysis: An excel based program for the analysis of intracellular
556 calcium transients including multiple, simultaneous regression analysis. Comput Methods
557 Programs Biomed 113. https://doi.org/10.1016/j.cmpb.2013.09.004

558 Greensmith, D.J., Galli, G.L.J., Trafford, A.W., Eisner, D.A., 2014a. Direct measurements of SR free
559 Ca reveal the mechanism underlying the transient effects of RyR potentiation under
560 physiological conditions. Cardiovasc Res 103. https://doi.org/10.1093/cvr/cvu158

561 Greensmith, D.J., Galli, G.L.J., Trafford, A.W., Eisner, D.A., 2014b. Direct measurements of SR free
562 Ca reveal the mechanism underlying the transient effects of RyR potentiation under
563 physiological conditions. Cardiovasc Res 103. https://doi.org/10.1093/cvr/cvu158

564 Jaiswal, G., Kumar, P., 2022. Neuroprotective role of apocynin against pentylenetetrazole kindling
565 epilepsy and associated comorbidities in mice by suppression of ROS/RNS. Behavioural Brain
566 Research 419. https://doi.org/10.1016/j.bbr.2021.113699

567 Khatib, R., Wilson, F., 2018. Pharmacology of Medications Used in the Treatment of
568 Atherosclerotic Cardiovascular Disease, in: Encyclopedia of Cardiovascular Research and
569 Medicine. https://doi.org/10.1016/b978-0-12-809657-4.99756-4

570 LaCombe, P., Lappin, S.L., 2020. Physiology, Afterload Reduction, StatPearls.

571 Loyola, L.A., Pedreros, S., Morales, G., 1985. Para-hydroxyacetophenone derivatives from Senecio-
572 Graveolens. Phytochemistry 24, 1600–1602. https://doi.org/10.1016/s0031-9422(00)81074-2

573 Murphy, T. v., Kanagarajah, A., Toemoe, S., Bertrand, P.P., Grayson, T.H., Britton, F.C., Leader, L.,
574 Senadheera, S., Sandow, S.L., 2016. TRPV3 expression and vasodilator function in isolated
575 uterine radial arteries from non-pregnant and pregnant rats. Vascul Pharmacol 83.
576 https://doi.org/10.1016/j.vph.2016.04.004

577 Paredes, A., Palacios, J., Quispe, C., Nwokocha, C.R., Morales, G., Kuzmicic, J., Cifuentes, F., 2016.
578 Hydroalcoholic extract and pure compounds from Senecio nutans Sch. Bip (Compositae)
579 induce vasodilation in rat aorta through endothelium-dependent and independent
580 mechanisms. J Ethnopharmacol 192. https://doi.org/10.1016/j.jep.2016.07.008

581 Pires, P.W., Sullivan, M.N., Pritchard, H.A.T., Robinson, J.J., Earley, S., 2015. Unitary TRPV3 channel
582 ca2+ influx events elicit endothelium-dependent dilation of cerebral parenchymal arterioles.
583 Am J Physiol Heart Circ Physiol 309. https://doi.org/10.1152/ajpheart.00140.2015

584 Reuter, H., Pott, C., Goldhaber, J.I., Henderson, S.A., Philipson, K.D., Schwinger, R.H.G., 2005. Na+-
585 Ca2+exchange in the regulation of cardiac excitation-contraction coupling. Cardiovasc Res.
586 https://doi.org/10.1016/j.cardiores.2005.04.031

587 Schotola, H., Sossalla, S.T., Renner, A., Gummert, J., Danner, B.C., Schott, P., Toischer, K., 2017. The
588 contractile adaption to preload depends on the amount of afterload. ESC Heart Fail 4.
589 https://doi.org/10.1002/ehf2.12164

590 Surcel, A., Ng, W.P., West-Foyle, H., Zhu, Q., Ren, Y., Avery, L.B., Krenc, A.K., Meyers, D.J., Rock,
591 R.S., Anders, R.A., Meyers, C.L.F., Robinson, D.N., 2015. Pharmacological activation of myosin
592 ii paralogs to correct cell mechanics defects. Proc Natl Acad Sci U S A 112.
593 https://doi.org/10.1073/pnas.1412592112

594 Trafford, A.W., Díaz, M.E., Eisner, D.A., 1999. A novel, rapid and reversible method to measure Ca
595 buffering and time- course of total sarcoplasmic reticulum Ca content in cardiac ventricular
596 myocytes. Pflugers Arch 437. https://doi.org/10.1007/s004240050808

597 Varro, A., Negretti, N., Hester, S.B., Eisner, D.A., 1993. An estimate of the calcium content of the
598 sarcoplasmic reticulum in rat ventricular myocytes. Pflugers Arch 423.
599 https://doi.org/10.1007/BF00374975

600 Villagrán, C., Romo, M., Castro, V., 2003. Etnobotánica del Sur de los Andes de la primera región de
601 Chile: Un enlace entre las culturas altiplánicas y las de quebradas altas del Loa superior.
602 Chungará (Arica) 35. https://doi.org/10.4067/s0717-73562003000100005

603

Figure 1

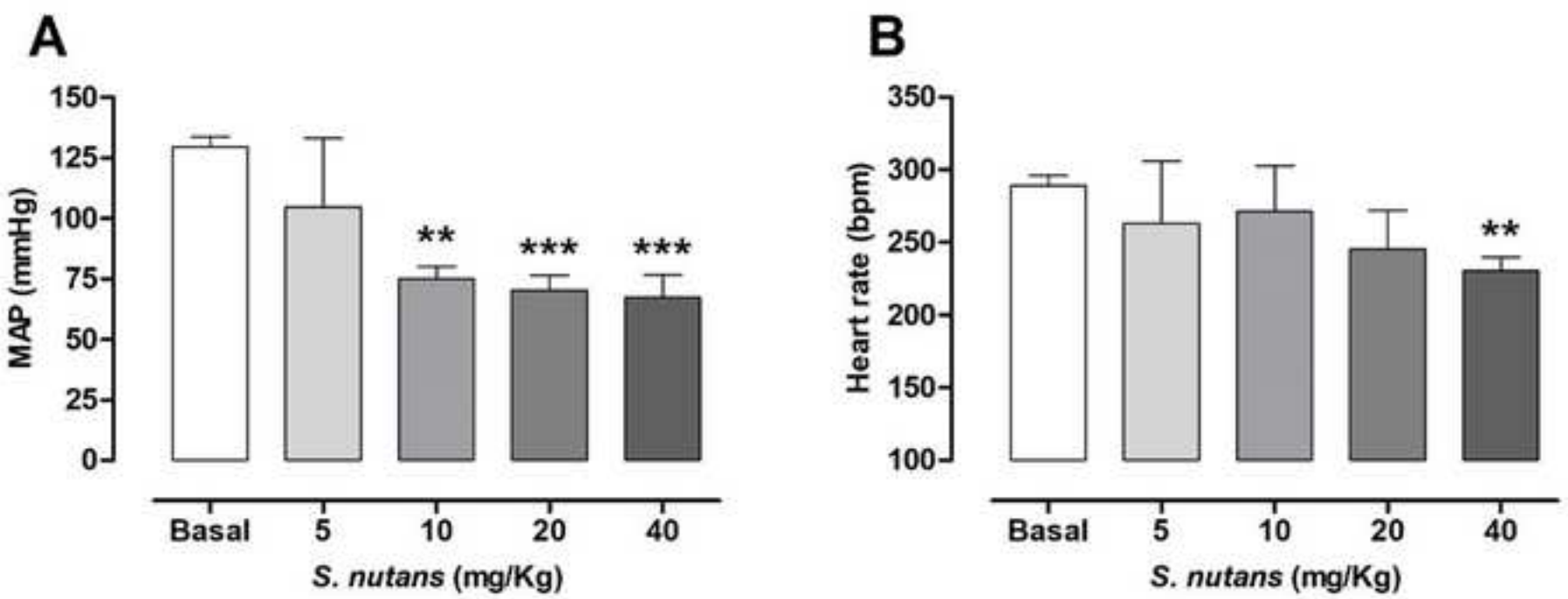

Figure 2

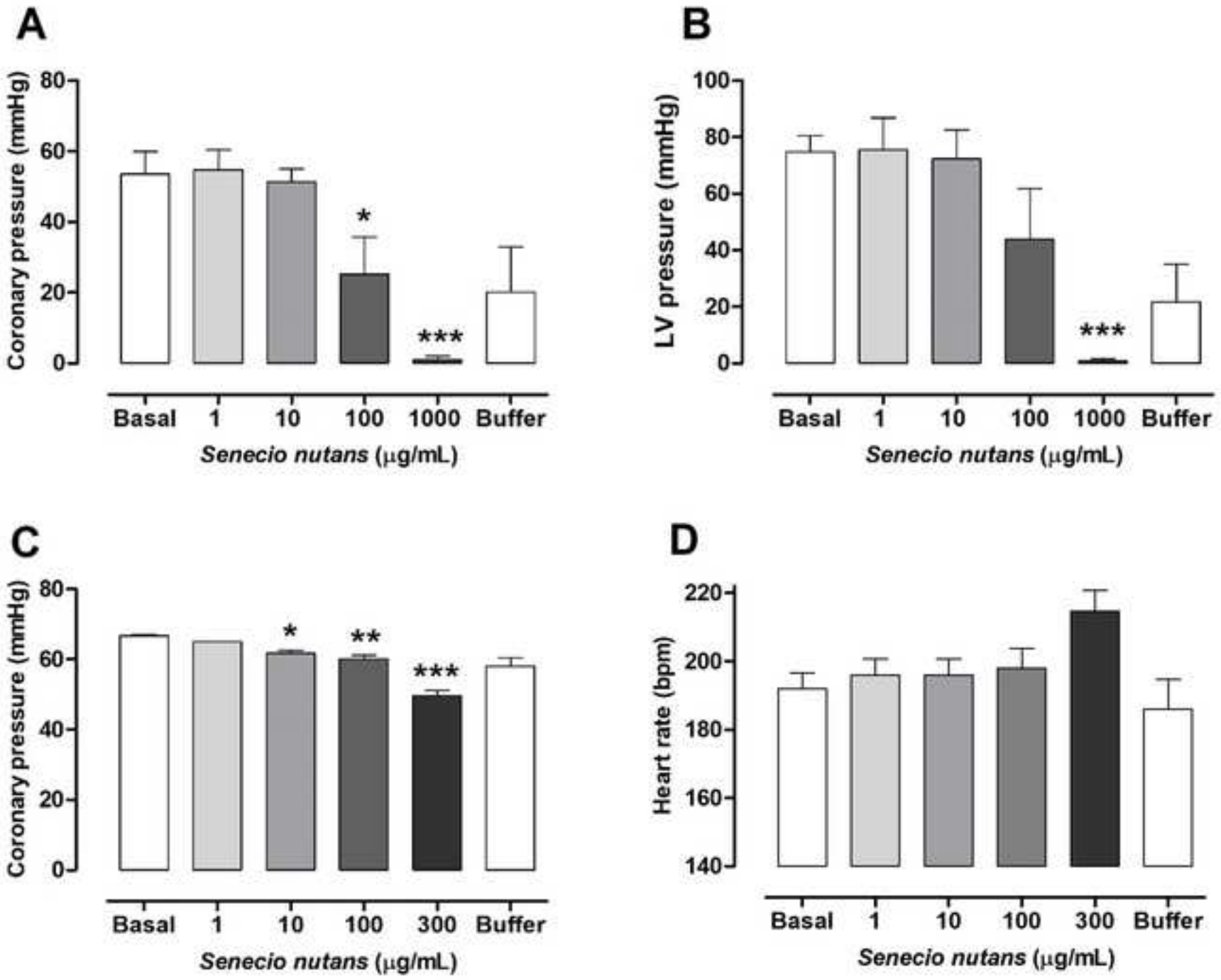

Figure 3

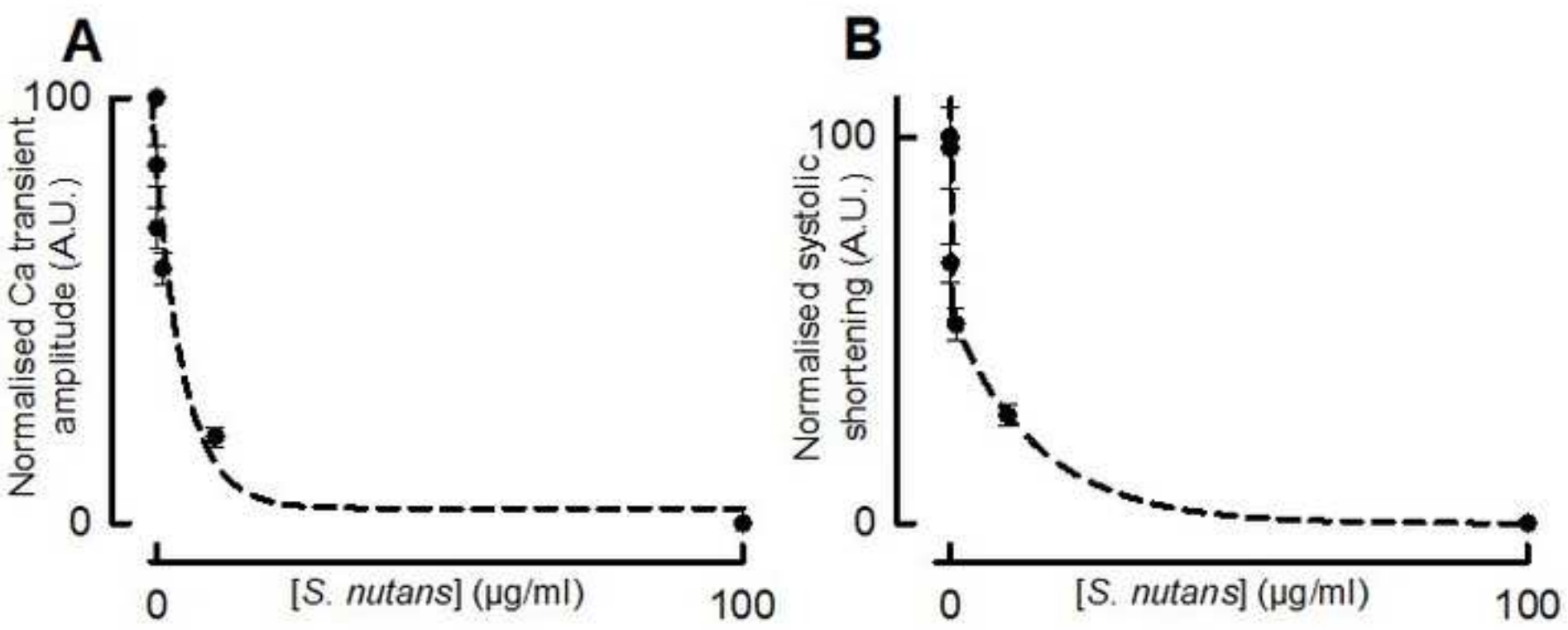

Figure 4

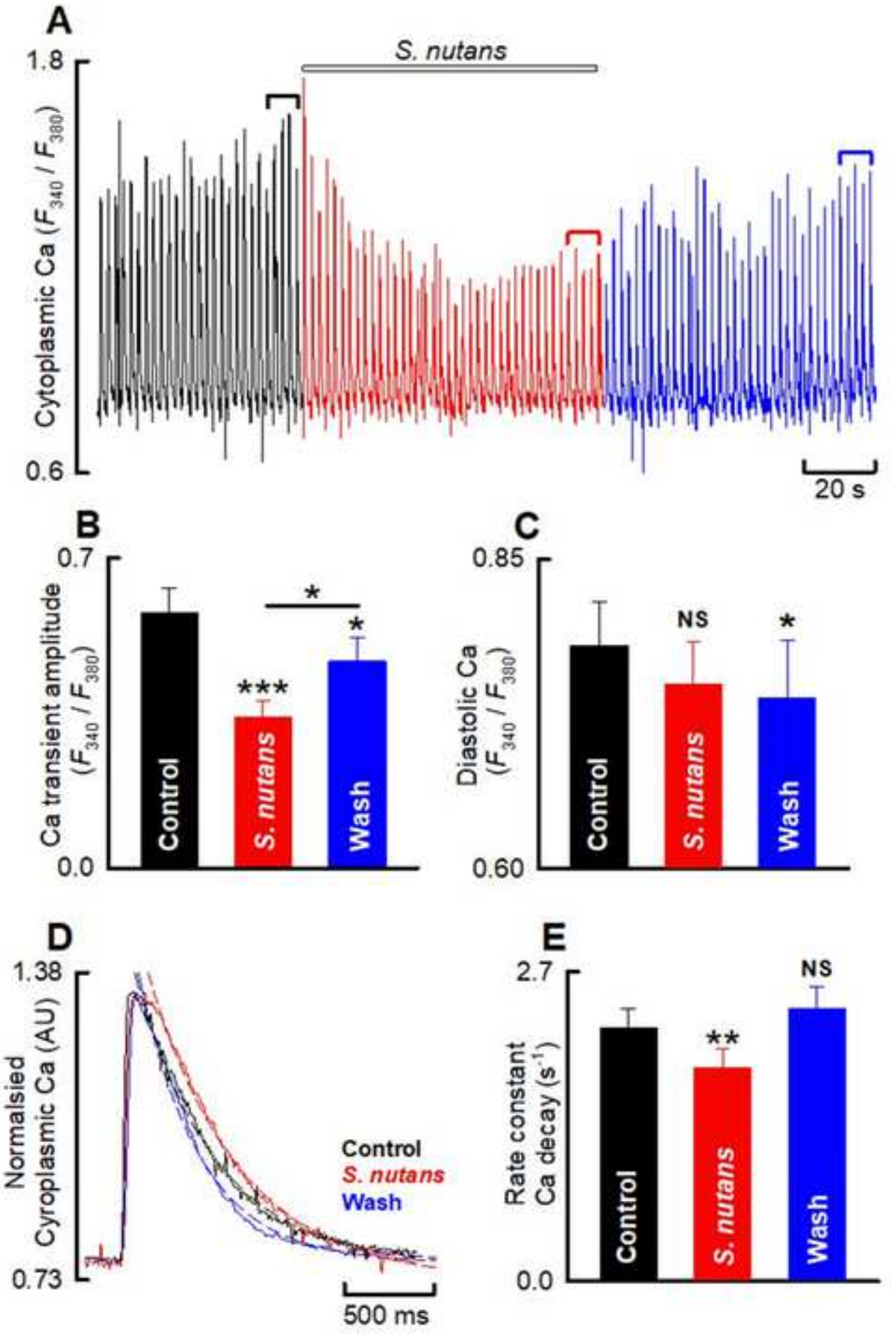

Figure 5

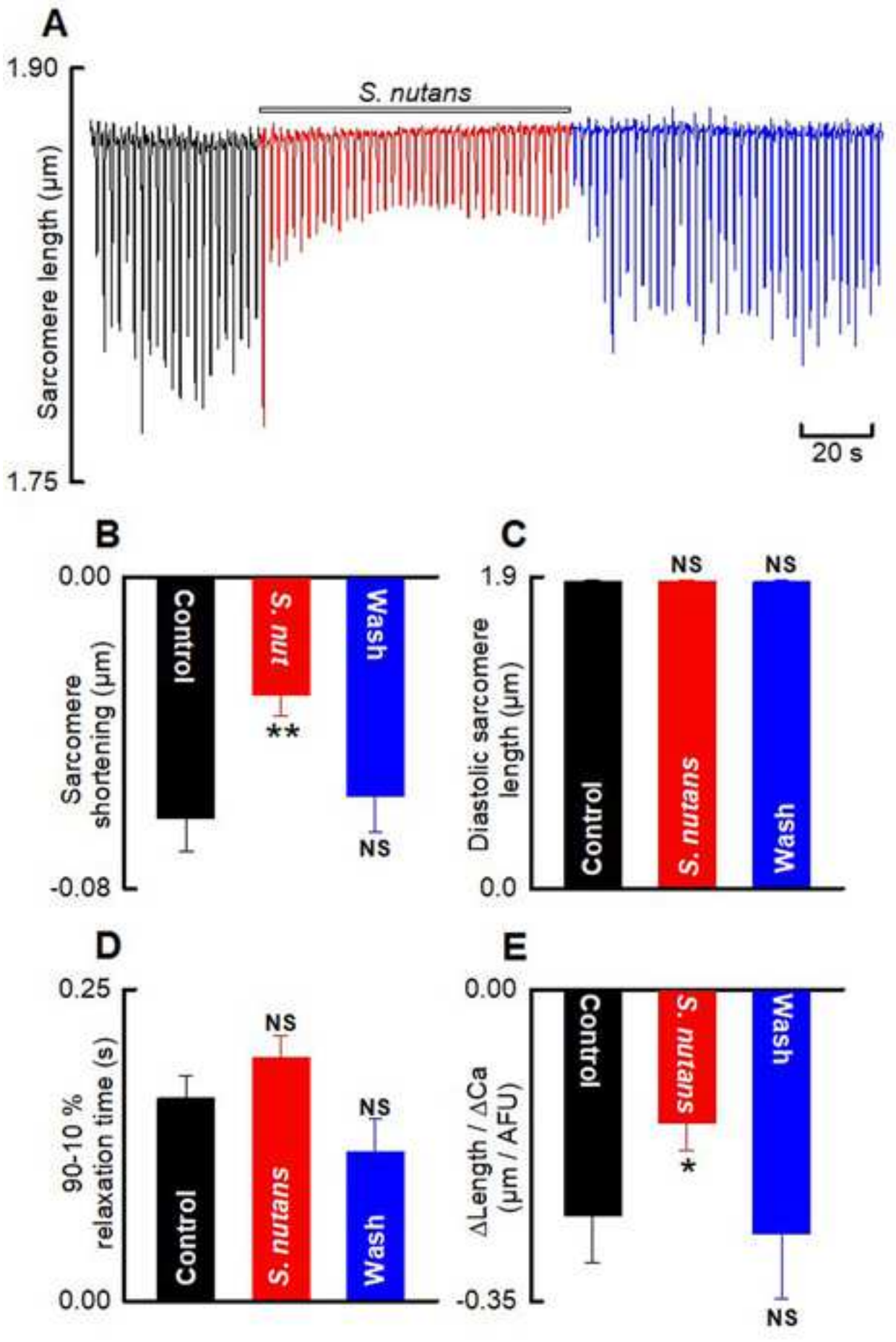

Figure 6

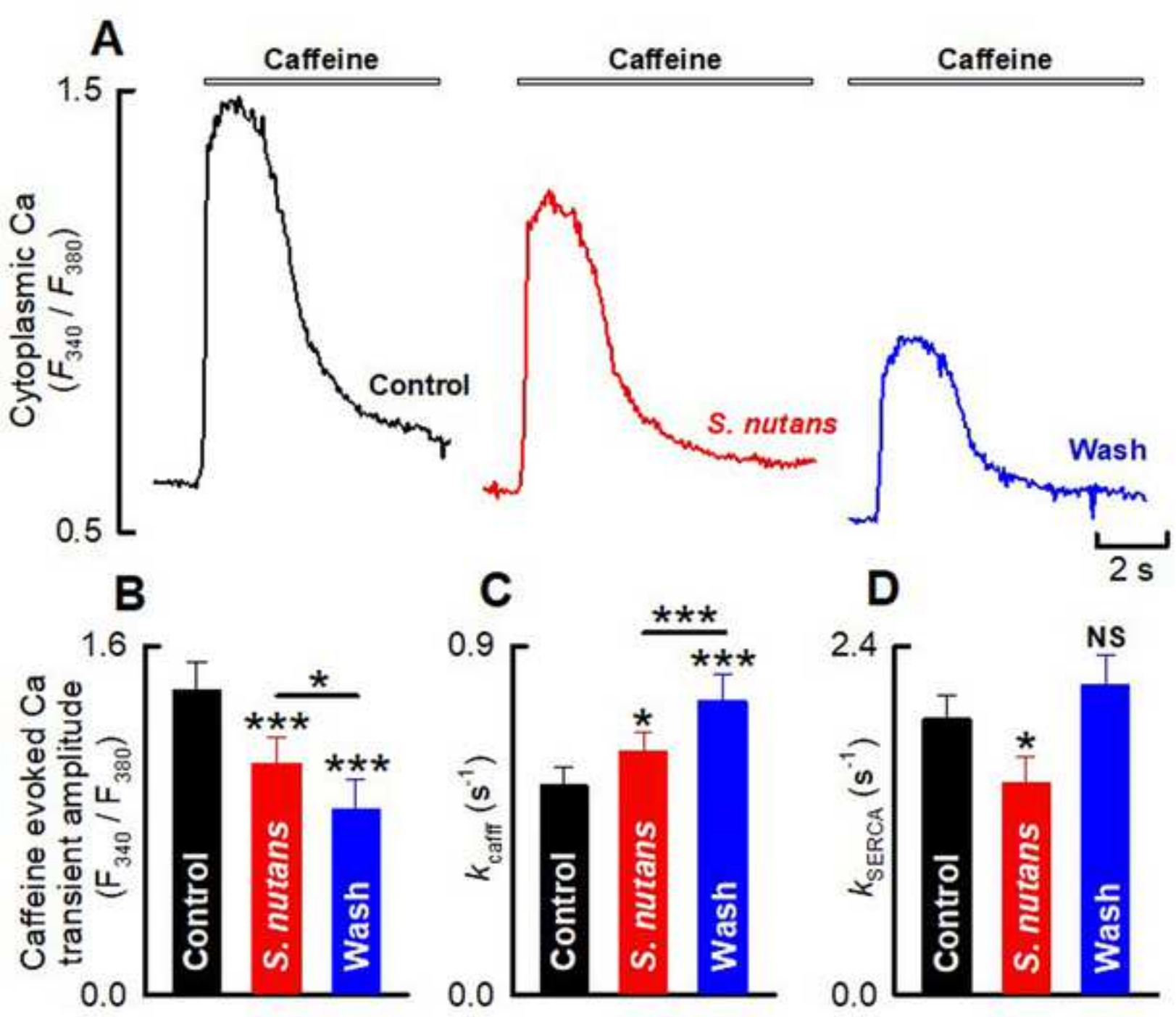

Figure 7

Click here to access/download;Figure;Fig 7.jpg